Author Manuscript

Author Manuscript

Author Manuscript

Author Manuscript

HHS Public Access

Author manuscript

Nature. Author manuscript; available in PMC 2014 December 05.

Published in final edited form as:

Nature. 2014 June 5; 510(7503): 115–120. doi:10.1038/nature13413.

miR-34/449 miRNAs are required for motile ciliogenesis by repressing *cp110*

Rui Song[1,*,#], **Peter Walentek**[2,*], **Nicole Sponer**[1,*], **Alexander Klimke**[3], **Joon Sub Lee**[1], **Gary Dixon**[1], **Richard Harland**[2], **Ying Wan**[4], **Polina Lishko**[1], **Muriel Lize**[5], **Michael Kessel**[3], and **Lin He**[1,#]

[1]Division of Cellular and Developmental Biology, MCB department, University of California at Berkeley, Berkeley, CA 94705, USA

[2]Division of Genetics, Genomics and Development, Centre for Integrative Genomics, MCB department, University of California at Berkeley, Berkeley, CA 94705, USA

[3]Department of Molecular Cell Biology, Max Planck Institute for Biophysical Chemistry, Goettingen, Germany

[4]The third Military Medical University, Chongqing, China

[5]Department of Molecular Oncology, University of Goettingen, Goettingen, Germany

Summary

The *miR-34/449* family consists of six homologous miRNAs at three genomic loci. Redundancy of *miR-34/449* miRNAs and their dominant expression in multiciliated epithelia suggest a functional significance in ciliogenesis. Here, we report that mice deficient for all *miR-34/449* miRNAs exhibited postnatal mortality, infertility, and strong respiratory dysfunction caused by defective mucociliary clearance. In both mouse and *Xenopus*, *miR-34/449*-deficient multiciliated cells (MCCs) exhibited a significant decrease in cilia length and number, due to defective basal body maturation and apical docking. The effect of *miR-34/449* on ciliogenesis was mediated, at least in part, by post-transcriptional repression of Cp110, a centriolar protein suppressing cilia assembly. *cp110* knockdown in *miR-34/449*-deficient MCCs restored ciliogenesis by rescuing basal body maturation and docking. Altogether, our findings elucidate conserved cellular and molecular mechanisms through which *miR-34/449* regulate motile ciliogenesis.

Users may view, print, copy, and download text and data-mine the content in such documents, for the purposes of academic research, subject always to the full Conditions of use:http://www.nature.com/authors/editorial_policies/license.html#terms

[#]Correspondence and requests for materials should be addressed to LH (lhe@berkeley.edu) and RS (rui.song@berkeley.edu).
[*]These authors contributed equally.

Author contributions: RS identified and characterized PCD-like motile cilia defects in *miR-34/449* TKO mice, defined *miR-34/449* expression in ciliated epithelia, identified and validated Cp110 as a key *miR-34/449* target in mice. PW contributed all *Xenopus* data, in particular, provided functional data validating Cp110 as a key *miR-34/449* target. NS performed all immunofluorescence experiments in mice, and contributed to target validation experiments. RS and PW both made significant contribution to experimental planning and result interpretation. ML, AK and MK generated and characterized *mir-449* KO mice, defined *miR-449* expression patterns in mouse embryos, and contributed to the revision of the manuscript. JSL and GD contributed to histology analyses and RT-QPCR analyses. PL contributed to the high-speed imaging experiments. WY characterized *miR-34/449* expression in human respiratory epithelia. RH contributed to the interpretation of data and to manuscript preparation. LH generated *mir-34a* and *mir-34b/34c* KO mice, interpreted the data and coordinated with different groups to complete this study. RS, PW, NS and LH are the major contributors to the preparation of this manuscript.

Author Manuscript Author Manuscript Author Manuscript Author Manuscript

Introduction

microRNAs (miRNAs) encode a class of small, non-coding RNAs that regulate gene expression through post-transcriptional repression[1–4]. Although the initial discovery of miRNAs was made through classic forward genetics in worm development[5,6], loss-of-function studies on most individual miRNAs yield no overt developmental defects in multiple organisms, suggesting strong functional redundancy among homologous miRNAs[7,8]. Redundant miRNAs can be generated from multiple genomic loci or transcribed from a single polycistronic precursor. Collectively, homologous miRNAs could constitute the majority of expressed miRNAs in specific cell types[9,10]. Such extensive homology and dominant cell-type specific expression of a single miRNA family could confer a robust functional readout that can only be revealed by complete removal of redundant miRNAs.

miR-34/449 miRNAs constitute a conserved family in vertebrates[11–13], comprising three genomic loci, *mir-34a*, *mir-34b/34c* and *mir-449c/449b/449a* (*mir-449*), which encode six homologous miRNAs (*miR-34a*, *34b*, *34c*, *449a*, *449b* and *449c*)[14,15] (Figure 1a, Extended Data Figure 1a). Sequence homology among *miR-34/449* miRNAs, particularly at the seed region, predicts robust functional redundancy. *miR-34/449* miRNAs are highly enriched in mucociliary epithelia that contain motile cilia[10], which beat coordinately to mediate fluid movement[16,17]. Structural and functional defects in motile cilia are associated with a human syndrome, primary cilia dyskinesia (PCD)[16,17]. Here, we demonstrate that *miR-34/449*-deficient mice developed PCD-like respiratory and fertility phenotypes. Consistently, *miR-34/449* deficiency in mice and frogs disrupts ciliogenesis in mucociliary epithelia, causing reduced cilia length and number due to impaired basal body maturation and apical docking. This is, at least in part, mediated by direct *miR-34/449* repression of Cp110, a centriolar protein suppressing cilia assembly[18,19]. These findings reveal conserved cellular and molecular mechanisms underlying the functions of *miR-34/449* in MCC ciliogenesis.

Results

PCD-like phenotype in *miR-34/449* TKO mice

To characterize *miR-34/449* functions, we generated triple knock-out (TKO) mice deficient for all *miR-34/449* loci (*mir-34a*, *mir-34b/34c*, and *mir-449*)[20] (Extended Data Figure 1b, 1c). Although *mir-449* resides in intron 2 of *cdc20b*[21], *mir-449* deletion in mice does not negatively impact *cdc20b* expression (not shown). TKO mice were born at a Mendelian ratio with normal body weight (Figure 1b, Extended Data Figure 1d); yet exhibited frequent postnatal mortality with only ~40% surviving to adulthood (Figure 1b). TKO mice also exhibited growth attenuation with ~50% lower body weight than littermate-controlled double knockout (DKO) mice (*mir-34a*$^{-/-}$*; mir-34b/34c*$^{-/-}$ or *miR-34a*$^{-/-}$*; mir-449*$^{-/-}$, Figure 1c, Extended Data Figure 1d).

Surviving TKO mice showed severe respiratory distress characterized by frequent coughing and sneezing (Extended Data Figure 1e, Video 1). Dying and surviving TKO mice displayed respiratory dysfunction, with excessive mucus accumulation in the paranasal cavities and increased susceptibility to respiratory infections (Figure 1d, Extended Data Figure 1f). Littermate-controlled *mir-34a*$^{-/-}$*; mir-34b/34c*$^{-/-}$ or *mir-34a*$^{-/-}$*; mir-449*$^{-/-}$ DKO mice

Author Manuscript Author Manuscript Author Manuscript Author Manuscript

phenotypically resembled wild-type mice, without obvious developmental or respiratory defects (Figure 1d, Extended Data Figure 1f, 1g).

Unlike phenotypically normal DKO controls (*mir-34a*$^{-/-}$*; mir-449*$^{-/-}$ or *mir-34a*$^{-/-}$*; mir-34b/34c*$^{-/-}$), surviving TKO males and females were infertile, generating no pregnancies when mated with wild-type animals. TKO males exhibited defective spermatogenesis during differentiation from elongating spermatids to spermatozoa (Figure 1e, Extended Data Figure 2a, 2b), when flagella formation occurs[17]. TKO females exhibited a decrease in fallopian tube epithelium ciliation, presumably causing defects in oocyte transport[17] (Figure 1e, Extended Data Figure 2a, 2c). Altogether, the TKO mouse phenotype resembled symptoms of a subset of PCD patients, exhibiting predominant respiratory and fertility defects without hydrocephaly or left-right asymmetry defects[22,23] (Extended Data Figure 2d).

Ciliogenesis defects in *miR-34/449* TKO mice

Mature *miR-34/449* miRNAs were enriched in organs containing motile cilia, including lung, brain, testis and female reproductive organs (Extended Data Figure 3a). We specifically detected and quantified individual *miR-34/449* miRNAs using single knock-out and TKO controls (Figure 2a, Extended Data Figure 3b, 3c). *In situ* hybridization revealed high-level *miR-34/449* expression in respiratory epithelia, with *miR-34a* being expressed broadly in multiple cell types, and *mir-34c* or *miR-449c* being enriched specifically in airway MCCs (Figure 2a, Extended Data Figure 3d).

A major consequence of PCD is dysfunctional airway clearance[16,17]. Defective mucociliary clearance in *miR-34/449* TKO mice, along with the MCC-specific *miR-34/449* expression, prompted us to examine the roles of *miR-34/449* in airway MCCs. High-speed imaging revealed a slow and limited fluid movement in TKO tracheal explants, accompanied by a significant reduction of visibly ciliated MCCs (Figure 2b, Extended Data Video 2). This contrasts the effective anteriorward fluid flow in wild-type and DKO tracheal explants (Figure 2b, Extended Data Video 2, 3).

The decrease of visible MCCs in TKO tracheas could reflect defective cell fate specification or ciliogenesis. We analyzed *mir-34a*$^{-/-}$; *mir-449*$^{-/-}$ DKO and TKO tracheas for Foxj1, a master regulator of motile ciliogenesis[24], and Acetylated α-tubulin (Ac-α-tub), a cilia marker. Both DKO and TKO tracheas had Foxj1 immunofluorescence staining and *foxj1* mRNA levels comparable to wild-type controls (Figure 2c, Extended Data Figure 3e). Nevertheless, a portion of Foxj1-positive cells lacked cilia in TKO tracheas, yet most Foxj1-positive cells were fully ciliated in DKO and wild-type tracheas (Figure 2c, not shown). This suggests normal cell fate specification with defective ciliation in *miR-34/449*-deficient MCCs. Scanning electron microscopy supported this finding, revealing a significant reduction in cilia length and number per MCC in TKO, but not DKO and wild-type tracheal epithelia (Figure 2d, Extended Data Figure 3f). Notably, TKO MCCs displayed a spectrum of ciliation phenotypes (non-ciliated, partially or fully ciliated; Figure 2d), possibly due to the mixed genetic background.

MCC ciliogenesis is characterized by the multiplication of basal bodies, which, after docking to the apical membrane, act as microtubule-organizing centers to assemble motile

Author Manuscript Author Manuscript Author Manuscript Author Manuscript

axonemes[25,26]. We stained TKO tracheas with antibodies against Ac-α-tub and γ-tubulin (γ-tub) to visualize cilia and basal bodies of MCCs, respectively. Consistent with previous observations, Ac-α-tub staining was greatly decreased in TKO tracheas, yet the percentage of γ-tub-enriched MCCs remained normal (Figure 3a, Extended Data Figure 4a, 4b). Air-liquid interface (ALI) culture of primary TKO tracheal epithelia yielded a similar observation (Extended Data Figure 4c). Thus, basal body multiplication occurred normally in *miR-34/449*-deficient MCCs following MCC cell fate specification, yet cilia formation was impaired.

Impaired basal body docking in *miR-34/449* TKO mice

Basal body docking to the apical MCC membrane is essential for proper ciliogenesis[25,26]. In *mir-34a*$^{-/-}$*; mir-34b/34c*$^{-/-}$ DKO MCCs, γ-tub staining was apically localized, indicating normal basal body docking (Figure 3b). In contrast, γ-tub staining was diffuse in TKO tracheal MCCs and ALI culture, suggesting defective basal body docking to or stabilization at the apical membrane (Figure 3b, Extended Data Figure 4d). Transmission electron microscopy revealed well-aligned basal bodies at the apical membrane of wild-type and DKO MCCs (Extended Data Figure 4e). Yet in TKO MCCs, a significant percentage of basal bodies were mislocalized to the cytoplasm and unable to grow cilia, and those apically docked generally formed shorter cilia (Figure 3c, 3d). The extent of ciliation defects correlated well with basal body docking defects, suggesting aberrant basal body docking as a key mechanism for impaired ciliation (Figure 3d). Defective ciliation and basal body docking in TKO MCCs also correlated with a disturbed subapical actin organization (Extended Data Figure 4f).

Despite defective basal body docking in TKO MCCs, the structural components of basal bodies, either apically docked or mislocalized, remained largely intact (Extended Data Figure 5a, 5b). While axoneme structure was unaffected in TKO MCCs, basal body orientation and ciliary axoneme directionality exhibited mild defects (Extended Data Figure 5c, 5d), which, in combination with the ciliation defects, likely evoked a strong mucociliary clearance phenotype.

miR34/449 functions in *Xenopus* MCCs

Mammalian and *Xenopus miR-34/449* miRNAs are not only conserved in sequence[14,15], but also in MCC-specific expression and ciliogenesis[10]. As a mucociliary epithelium, the *Xenopus* embryonic epidermis resembles mammalian airway epithelia in MCC development and function[27]. As in mouse, knock-down of *Xenopus miR-34a/34b/449a* by morpholino injection (*miR-34/449* MOs) reduced cilia number and length in tadpole epidermal MCCs (Figure 4a, 4b). No obvious defects in embryonic development, hydrocephalus, MCC cell fate specification, or other cell type specification were observed (Extended Data Figure 6a-f). In *miR-34/449* morphants, a significant portion of MCCs were either partially ciliated (>50%), or devoid of cilia (29%±17%), with frequent, unorganized subapical Ac-α-tub enrichment indicating defective basal body docking[28] (Figure 4b). Consistently, basal bodies detected by γ-tub or Sas6-GFP[29] exhibited irregular distribution and frequently failed to form cilia in *miR-34/449*-deficient MCCs (Figure 4c, Extended Data Figure 6g).

Author Manuscript Author Manuscript Author Manuscript Author Manuscript

miR-34/449 miRNAs directly repress *cp110* in MCCs

miR-34/449 increase during MCC differentiation[30] predicts a decrease of functionally important targets, which invariably contain *miR-34/449* binding site(s) in the 3′ untranslated region (3′UTR)[31,32]. We analysed published gene expression profiles of tracheal MCCs during differentiation[30,33], then selected 57 potential *miR-34/449* targets for RT-QPCR validation in DKO and TKO tracheas, and finally narrowed down to those with important ciliogenesis functions (Extended Data Table 1). *cp110* emerged as a strong candidate, containing two *miR-34/449* binding sites (Extended Data Figure 7a), and exhibiting *miR-34/449*-dependent repression *in vivo* and in luciferase assays (Figure 5a, 5b, Extended Data Figure 7b, 7c).

Cp110 is a distal centriolar protein suppressing primary cilia assembly[18,19]. Aberrant Cp110 retention in mother centrioles is correlated with impaired basal body docking[34]. In addition to its well-characterized roles in primary cilia, Cp110 is also implicated as an important regulator of motile ciliogenesis[35,36].

miR-34/449 and *cp110* are conserved in mice and frogs. *Xenopus cp110* contains one predicted *miR-34/449* binding site (Extended Data Figure 7d), suggesting a selective pressure to preserve *miR-34/449-cp110* regulation. *miR-34/449* and *cp110* levels are inversely correlated during MCC differentiation in *Xenopus*; and *cp110* mRNA was derepressed in *miR-34/449* morphants (Extended Data Figure 7e-g). Strikingly, *cp110* knockdown in *miR-34/449* deficient MCCs significantly rescued ciliation defects (Figure 5c, Extended Data Figure 8a, 8b).

We subsequently examined, in control and *miR-34/449* morphants, the localization of Centrin4[37], an important basal body component whose loss-of-function causes a PCD-like phenotype[38]. While strong Centrin4-foci were enriched apically in controls, these foci significantly decreased in intensity and failed to localize to the apical membrane of *miR-34/449*-deficient MCCs (Figure 5d, Extended Data Figure 8c). These findings demonstrated defective basal body docking and decreased basal body incorporation of Centrin4 in *miR-34/449*-deficient MCCs, both of which were rescued by co-injection of *cp110* MO (Figure 5d).

Consistently, *cp110* overexpression generally phenocopied *miR34/449* knockdown, causing impaired ciliation and decreased Centrin4 incorporation into basal bodies, without affecting MCC cell fate specification or subapical actin organization (Figure 5c, Extended Data Figure 8b, 8d-e, 9a). *cp110* with a 3′UTR deletion exhibited a stronger phenotype than full-length *cp110*, suggesting *cp110* repression by *miR34/449* even during overexpression (Extended Data Figure 7d, 8b, 8d). Surprisingly, *cp110* MO injection alone also gave rise to reduced cilia number and length, and aberrant basal body aggregation in MCCs (Figure 5c, Extended Data Figure 8a, 8b, 9b). Thus, *miR-34/449* miRNAs mediate precise Cp110 regulation during vertebrate MCC ciliogenesis (Figure 5e).

Author Manuscript Author Manuscript Author Manuscript Author Manuscript

Discussion

miR-34/449 represent the first non-coding RNAs whose deficiency causes a PCD-like airway and fertility phenotype. *miR-34* miRNAs have been mostly characterized as p53 targets that elicit multiple tumour suppressor effects[20,39]; yet the MCC-specific *miR-34/449* expression and functions are likely p53-independent (not shown). While most characterized PCD mutations affect structural components of the ciliary axoneme[17,40] or basal body structure[41], *miR-34/449* miRNAs regulate ciliogenesis by promoting basal body maturation and docking without affecting overall structure. Interestingly, redundant *miR-34/449* miRNAs are not functionally equivalent in mice. One *mir-34b/34c* or *mir-449* allele is sufficient for proper MCC ciliation; two intact *mir-34a* alleles in *mir-34b/34c*$^{-/-}$*; mir-449*$^{-/-}$ DKO mice still yield clear respiratory and fertility phenotypes (not shown). Distinct roles of *miR-34/449* miRNAs could reflect differential expression rather than target specificities.

In a previous study, *miR-449* inhibition alone caused defective ciliogenesis by derepressing Notch1 and Dll1[10]. Yet normal MCC specification in *miR-34/449*-deficient MCCs suggest that Notch pathway components, with well-characterized roles in regulating MCC differentiation[42,43], may not act as key *miR-34/449* targets in motile ciliogenesis. Here, we provide molecular and functional evidence demonstrating *cp110* as a major *miR-34/449* target. Cp110 levels have to be tightly regulated spatially and temporally during MCC ciliogenesis; and proper Cp110 removal from mother centrioles is essential for ciliation[19]. Previous studies mostly focused on ubiquitin-mediated proteasomal degradation of Cp110[44,45]. Our study revealed the important post-transcriptional regulation of Cp110 by *miR-34/449*. While MCC-enriched *miR-34/449* miRNAs repress *cp110* to facilitate ciliation, other miRNAs (e.g. *miR-129*) repress *cp110* expression in other cell types to regulate ciliogenesis of primary or motile mono-cilia[36]. Thus, ciliogenesis is controlled by downregulation of *cp110* through distinct miRNAs in distinct cell types.

For miRNAs, their small size and imperfect target recognition facilitate regulation of multiple mRNA targets. Here, *cp110* knockdown restored basal body maturation / docking and ciliogenesis in *miR-34/449*-deficient MCCs; yet additional *miR-34/449* targets likely exist to regulate the organization of the subapical actin cytoskeleton in MCCs.

Mucociliary epithelia are morphologically and functionally conserved among vertebrates[27]. Our findings demonstrated a conserved mechanism that regulates basal body maturation and docking in MCCs by *miR-34/449*-dependent fine-tuning of Cp110 levels. This mechanism could have profound implications for the underlying mechanisms disrupted in patients with PCD-like syndromes.

Methods

Mouse breeding, genotyping and monitoring

mir-34a$^{-/-}$; *mir-34b/34c*$^{+/-}$; *mir-449*$^{-/-}$ intercross mating and mir-*34a*$^{-/-}$; *mir-34b/34c*$^{-/-}$; *mir-449*$^{+/-}$ intercross mating were both established to generate *miR-34/449* triple knockout (TKO) mice. TKO mice were generated on a mixed genetic background containing C57BL/6, 129 and CD1, and were subsequently backcrossed to C57BL/6 for at least four

Author Manuscript Author Manuscript Author Manuscript Author Manuscript

generations. All mice were housed in a non-barrier animal facility at UC-Berkeley. The following primers were used for genotyping, with parenthetical values indicating the size of the diagnostic PCR product: *mir-34a*-Common-R, ACTGCTGTACCCTGCTGCTT, with *mir-34a*-WT-F, GTACCCCGACATGCAAACTT (wild-type band, 400 bp), or *mir-34a*-KO-F, GCAGGACCACTGGATCATTT (KO band, 263 bp); *mir-34b/34c*-Common-R, GAGATTTTCGTGGCGCTTTA, with *mir-34b/34c*-WT-F, GCCTCCTGTGAATCGTCATT (wildtype band, 264 bp), or *mir-34b/34c*-KO-F, GCGGCCGCATAACTTCGTAT (KO band, 155 bp);. *mir-449*-Common-R, ACATCCCCAAGATATCCCA, with *mir-449*-WT-F, GTATCCACGCCACCACA (wild-type band, 724 bp), or *mir-449*-KO-F, GAGTTTTCTGGGCTTGCC, (KO band, 406 bp). Litters were monitored daily for the first 60 days for survival, and their body weight was measured every other day for the first 30 days. The sound wave analyses were performed using audios that recorded the TKO phenotypes (Extended Data Video 1); and respiratory sound was analyzed using Audacity.

Histological analyses

Tissues were dissected and fixed overnight in 10% neutral buffered formalin, pH 7.4 (NBF) (Fisher Scientific, #SF100-4), processed by standard procedures, and embedded in paraffin blocks. All the blocks were sectioned at 10 μm, and slides were stained by hematoxylin and eosin (H & E). In this analysis, lungs were inflated via trachea with 10% NBF prior to fixation; and sinuses were processed by post-fixation decalcification for 5 to 10 days in 10% EDTA, pH 7.0.

Real time QPCR

Total RNA was isolated by Trizol (Invitrogen, #15596) from tracheal epithelium per the manufacturer's protocol, and treated with DNase I (Invitrogen, #18068) to remove DNA contamination. For quantitation of mRNAs, Trizol prepared RNA was reversely transcribed into cDNA using SuperScript III reverse transcriptase (Invitrogen, #18080) with random primers. SYBR Green-based QPCR was subsequently performed on a 7900HT real-time PCR system (Applied Biosystems) using cDNA as template. The *gpdh*-encoding transcript was used as an endogenous control in each QPCR. The following QPCR primers were used in this study, with parenthetical values indicating the size of the diagnostic PCR product: *cp110*-F: TCTCCACTGCTTACCATTGA, and *cp110*-R: GTAAATGGTTTCTGTTGCCC (195 bp); *foxj1*-F: CTCCTATGCCACTCTCATCT, and *foxj1*-R: GGATGGAATTCTGCCAGGTG (137 bp); *gapdh*-F: AACTTTGGCATTGTGGAAGG, and *gapdh*-R: CACATTGGGGGTAGGAACAC (222 bp). Four independent groups of mice were collected for RT-QPCR quantitation of *cp110* and *foxj1*. Each group contained a TKO mouse, an age-matched wild-type mouse, and a littermate-controlled DKO mouse (*mir-34a*$^{-/-}$; *mir-34b/34c*$^{-/-}$ or *mir-34a*$^{-/-}$; *mir-449*$^{-/-}$). For *Xenopus* RT-QPCR, cDNA was generated from total RNA extracts of skin explants using iScript Reverse Transcription Supermix (BioRad, # 170-8840); and the following QPCR primers were used: *Foxj1*-F: CCAGTGATAGCAAAAGAGGT, and *Foxj1*-R: GCCATGTTCTCCTAATGGAT; *Cp110*-F: AGCCAGAATCCAAGTAAAGG, and *Cp110*-R: CTTGCTTCTTTTCAGCAGTC; *EF1a*-F: CCCTGCTGGAAGCTCTTGAC, and *EF1a*-R: GGACACCAGTCTCCACACGA;

Author Manuscript Author Manuscript Author Manuscript Author Manuscript

ODC-F: GGGCTGGATCGTATCGTAGA, and *ODC*-R: TGCCAGTGTGGTCTTGACAT. Reactions were performed on a BioRad CFX96 Real-Time System C1000 Touch.

For miRNA quantitation, Trizol prepared total RNA was poly (A)-tailed by Poly (A) Polymerase (Epicentre, #PAP5104H). Poly (A)-tailed small RNA was reversely transcribed into small RNA cDNA with SuperScript III reverse transcriptase (Invitrogen, #18080) using miRNA RT primer (5′-CGAATTCTAGAGCTCGAGGCAGGCGACATGGCTGGCTAGTTAAGCTTGGTACCGAGCTCGGATCCACTAGTCCTTTTTTTTTTTTTTTTTTTTTTTVN-3′). (V is A, G or C; N is A, G, C or T). TaqMan-based QPCR was subsequently performed on a 7900HT fast real-time PCR system (Applied Biosystems). The U6 snRNA was used as the endogenous control for miRNA real time QPCR analyses. Universal TaqMan probe, CTCGGATCCACTAGTC; Universal reverse primer, CGAATTCTAGAGCTCGAGGCAG. The following forward primers, specific for each small RNA, were used in our studies: *miR-34a*, TGGCAGTGTCTTAGCTGGTTGT; *miR-34b*, AGGCAGTGTAATTAGCTGATTGT; *miR-34c*, AGGCAGTGTAGTTAGCTGATTGC; *miR-449a*, TGGCAGTGTATTGTTAGCTGGT; *miR-449b*, AGGCAGTGTTGTTAGCTGGC; *miR-449c*, AGGCAGTGCATTGCTAGCTGG; and U6 snRNA, CGCAAATTCGTGAAGCGTTCC. For *Xenopus* miRNA quantitation following primers were used: U6 snRNA: ATGTGAAGCGTTCCATATGA; *miR-34a*: TGGCAGTGTCTTAGCTGGTTGTT; *miR-34b*: CAGGCAGTGTAGTTAGCTGATTG; *miR449c*: TGCACTTGCTAGCTGGCTGT. Statistical evaluation was performed using paired t-test.

In situ hybridization (ISH)

Standard histology protocols were used to prepare P25 lung and trachea section for miRNA ISH using Diethylpyrocarbonate (DEPC) treated water for all procedures. After deparaffinization and rehydration, slides were fixed with 4% paraformaldehyde (PFA), treated with Proteinase K, and fixed again with 4% PFA. Slides were incubated first with pre-hybridization solution (3 to 4 hours at 60 °C), and then with hybridization solution mixed with digoxigenin (DIG) -labeled LNA probes against each *miR-34/449* miRNA (16 hours at 60 °C). Post hybridization, slides were washed for 10 minutes at 60 °C in a graded series of SSC solutions (2×, 1.5×, 0.2×), then incubated with alkaline phosphatase (AP)-conjugated anti-DIG antibody in blocking solution. After washing with PBS and alkaline phosphatase (AP) buffer, the slides were incubated with NBT/BCIP in AP buffer to visualize blue ISH signals. Nuclear fast red (Sigma, #N3020) was used for nuclear counter staining. Slides then were dehydrated and mounted with Permount (Fisher Scientific, #SP15-100). Solutions for ISH (BioChain #K2191020) as described above. DIG-labeled *miR-34a* (ACAACCAGCTAAGACACTGCCA), *miR-34c* (GCAATCAGCTAACTACACTGCCT), and *miR-449c* (CCAGCTAGCAATGCACTGCCT) probes were purchased from Exiqon (#38487-01, #38542-01, and #39641-01 respectively). For *Xenopus* ISH, embryos were fixed in MEMFA at the indicated stages, and standard protocols were used for ISH and bleaching of embryos[46]. *Foxj1* anti-sense probe[24] was synthesized using sp6 polymerase (Promega,

Author Manuscript Author Manuscript Author Manuscript Author Manuscript

#P1085). Whole mount ISH was performed on groups of 25 control and manipulated specimens per time point and batch, which were derived from two different mothers.

Visualization of ciliary beating and mucociliary transport

Trachea from adult mouse was cut into 2 mm × 2 mm pieces under dissection microscope. Trachea pieces then were transferred into the chamber on a glass slide, which was made by placing a 0.5-mm sticky spacer (Bio-Rad, #SLF-1201) on the slide surface. The chamber was filled with 100 μL M199 Hank's balanced salts medium (Invitrogen, #12350-039) mixed with 1 μL red fluorescent 0.5-μm microspheres (Invitrogen, # F-8812); and a cover glass was placed on the sticky spacer to seal the chamber. Live images of the tracheal epithelium were recorded with a high-speed GX-1 Memrecam camera (NAC Image Technology) attached to an Olympus IX71 microscope. DIC channel was used to record multiciliary beating, and the red fluorescent channel was used to record mucociliary transport. Videos were recorded at 250 frame per second (FPS) for 8 seconds, and are played at 250 FPS in Extended Data Video 2 and 3. Image J was used to process and analyze raw images (Extended Data Video 2, and 3).

Immunofluorescence staining and confocal imaging

For Immunofluorescence staining on cryosections, whole tracheas of adult mice were fixed overnight in ice-cold acetone, and then processed through a graded series of sucrose solutions (from 5% to 20%, Fisher Scientific, #S5-500). Tracheas were embedded in (1:1) 20% Sucrose and O.C.T. compound (Tissue-Tek, #4583) and sectioned with MICROM HM 550 (Fisher Scientific) at -21 °C at a thickness of 6 μm. Slides were washed in PBS (3× 15 min), blocked (1 hr at room temperature) in PBSTB (0.1% Triton X-100, 1% bovine serum albumin in PBS), and incubated (overnight at 4 °C) with primary antibodies (1:400, anti-*Foxj1*, Sigma HPA005714; 1:1000 anti-Acetylated-α-tubulin, Sigma T6793). sides then were washed three times in PBST (0.1% Triton X-100 in PBS), and incubated (1 hr at room temperature) with secondary antibody (1:1000, Cy3-goat-anti-mouse, Molecular Probes A10521 or 1:500 Alexa Fluor 488 goat anti-rabbit, Molecular Probes A11034). Slides were mounted with VECTASHIELD mounting medium with DAPI (Vector Laboratories, #H-1200). Images were taken with a Zeiss LSM 710 AxioObserver Inverted 34-Channel Confocal Microscope and analyzed with Zeiss Zen software.

For whole trachea staining, tracheas were cut longitudinally into two pieces, which were fixed either in 80% methanol (EMD, #M×0485P-4) with 20% DMSO (Fisher Scientific, #BP231-100) (overnight at -20 °C), or in 4% paraformaldehyde (PFA) (overnight at 4 °C), respectively. Fixed tissues were washed and blocked as described above, and then incubated (overnight at 4°C) with primary antibodies (1:500 anti-γ-tubulin, Sigma T5192 for the methanol fixed tissue; 1:400 anti-Foxj-1, Sigma HPA005714 and 1:1000 anti-acetylated-α-tubulin for the PFA fixed tissue). Tissue then was washed, incubated with secondary antibody, counterstained with DAPI, and imaged as described above.

For *Xenopus* MCC staining, immunofluorescence was performed on whole-mount embryos and skin explants fixed at embryonic stages 30-33 (unless specified otherwise) in 4% paraformaldehyde for 1-2 hr at room temperature[47] or in Dent's for 48 hr at -20°C. Embryos

Author Manuscript Author Manuscript Author Manuscript Author Manuscript

were processed according to standard procedures[46]. Morphological analysis of cell types was performed as previously descirbed[48]. Primary antibodies were as follows: mouse monoclonal anti-acetylated-α-tubulin (1:700; Sigma T6793); rabbit polyclonal anti-γ-tubulin (1:500; Sigma T5192). Secondary antibodies (1:250) were as follows: AlexaFlour 488-labeled goat anti-mouse antibody (Molecular Probes A11001), AlexaFluor 555-labeled goat anti-mouse antibody (Molecular Probes A21422), AlexaFluor 555-labeled goat anti-rabbit antibody (Molecular Probes A21428) and AlexaFluor 405-labeled goat anti-mouse antibody (Molecular Probes A31553). Actin staining was performed by incubation (30-60 min at room temperature) with AlexaFluor 488-labeled Phalloidin (1:40; Molecular Probes A12379). Z-stack analysis and processing were performed using Image J and Zeiss ZEN software. All confocal imaging was performed using a Zeiss LSM700.

Scanning Electron Microscopy (SEM)

Adult trachea tissue was fixed using Karnovsky's fixative in 0.1 M sodium phosphate buffer (Sorenson's), washed with Sorenson's sodium phosphate buffer and post-fixed using 1% OsO_4 in Sorenson's for 1 hour. Tissue was dehydrated by passaging through a graded series of ethanol solutions, then critical point dried using a Tousimis 931 Super Critical Point Dryer. The tissue was mounted on aluminum stubs and sputter coated with gold using a PELCO SC-7 coater. The samples were viewed on an FEI XL30 TMP SEM and digital images were collected. SEM was performed in the electron microscopy facility of the University of California at Davis.

Transmission Electron Microscopy (TEM)

Adult trachea tissue was fixed, washed, and post-fixed as for SEM. After rinsing in double-distilled water (DDW), the tissue was incubated (30 min at room temperature) in 0.1% tannic acid, rinsed again in DDW, and incubated (1 hr) in 1% uranyl acetate in DDW. Tissue was dehydrated by passaging through a graded series of acetone solutions, then infiltrated and embedded in an epoxy resin mixture. Survey thick sections were cut, and ultra-thin sections of the selected areas were generated with a diamond knife (Diatome). The thin sections were picked up on copper grids and stained with uranyl acetate and lead citrate before viewing on a Philips CM120 Biotwin. Micrographs were taken with a Gatan MegaScan Model 794/20 digital camera. TEM analyses with longitudinal and transverse sections were performed in the electron microscopy facility of the University of California at Davis. Image J was used to measure the distance between basal bodies and apical surface in TEM pictures, and Oriana was used to analyze the directionality of ciliary axonemes. The following criteria were used to determine multiciliated cells (MCCs) and their apical surface in longitudinal TEM: Cells containing basal bodies in tracheal epithelium were defined as MCCs. For ciliated MCCs, the surface with intact view from ciliary axoneme to basal body was determined as apical surface; and for non-ciliated MCCs, the surface with microvilli was determined as apical surface.

Air-Liquid Interface (ALI) culture of primary tracheal epithelia

Primary tracheal epithelial cells were cultured as described previously[49]. In short, tracheas from three adult *miR-34/449* mutant mice of the same genotype (~P60) were dissected and

Author Manuscript Author Manuscript Author Manuscript Author Manuscript

cut longitudinally in ice-cold Ham's F-12 medium (Life Technologies, #11765-054) with penicillin/streptomycin (Life Technologies, # 15140-163). To isolate epithelial cells, tracheas were incubated in 1.5mg/ml Pronase (Roche Diagnostics, #10165921001) in Ham's F-12 media overnight at 4°C. We stopped the tracheal Pronase digestion by adding fetal bovine serum (FBS, Omega Scientific, #FB-01) to a final concentration of 10%. The tracheas were washed twice in ice cold fresh Ham's F-12 media with 10% Fetal Bovine Serum (FBS). Tracheal epithelial cells were then pelleted by pooling the Pronase digestion and washes for centrifugation at 400× g for 10 min at 4 °C. The pelleted cells were treated by DNase I (Sigma, #DN25), resuspended in 1 mL FBS, then plated in 9 mL pre-warmed basic medium (BM), which contained 1:1 DMEM: Ham's F-12 (Life Technologies, #11330-032), penicillin/streptomycin, 1.5mM glutamine (Life Technologies, #25030-149), 0.03% sodium bicarbonate (Life Technologies, #25080-094), and 0.1% Fungizone (Life Technologies, #15290-018)). Fibroblasts were depleted by a four-hour incubation at 37 °C, after which the tracheal epithelial cells were plated on trans-wells (Corning, #3470) in 24-well plates in Proliferation Medium, which contained BM with 5% FBS, 25ng/ml Epidermal Growth factor (EGF) (BD Biosciences, #354001), 10μg/ml Insulin (Sigma, #I1882), 5 μg/ml apo-transferrin (Sigma, #T1147), 0.1 μg/ml cholera toxin extract (Sigma, #C8052), 30 μg/ml Bovine Pituitary Extract (BPE) (Hammond Cell Tech, #1078-NZ), and 50nM retinoic acid (RA, Sigma, #R2625-500MG). The Proliferation Medium was changed every other day for 7 days, until we switched the culture to air-liquid interface culture by removing the media in the apical chamber, and replacing the media in the basal chamber with Differentiation Medium (BM with 2% Nu-Serum (BD, #355100) and 50nM RA). The Differentiation Medium was changed every other day for 23 days, when cells were ready for IF staining.

Luciferase assay

A fragment of the *Cp110* mRNA 3′UTR containing two predicted *miR-34/449* sites was cloned into the FseI site immediately downstream of the stop codon in the pGL3-Control firefly *luciferase* vector (Promega, #E1741). We amplified a fragment of *Cp110* 3UTR using PCR with *Cp110*-3′UTR-F, AAGGCCGGCCGAAGACAGCACTCACTGGGA, and *Cp110*-3′UTR-R, GTGGCCGGCCTTCTCTGAGATCCGGATTGC. NIH/3T3 cells were cultured in 10% bovine serum in DMEM (Invitrogen, # 11995-073) in a 12-well plate at a density of 1×10^5 cells/well. We co-transfected each well of NIH3T3 cells with 10 ng of pGL3 constructs, 100 ng of pRL-TK *Renilla* vector (Promega, #E2241), and 15 nM *miR-34b* miRNA mimics (Integrated DNA Technologies, 5′ AGGCAGUGUAAUUAGCUGAUUGU 3′ and 5′ AAUCACUAACUCCACUGUUAUC 3′) or siGFP (Integrated DNA Technologies) using *Trans*IT-TKO Transfection Reagent (Mirus Bio, #MIR 2150). At 24 hours after transfection, firefly and *Renilla* luciferase activities were measured using the Dual-Luciferase reporter assay system (Promega, #E1910). The luciferase activity was normalized as the ratio of firefly/*Renilla* luciferase activities.

Western blotting

Protein was collected from mouse tracheal epithelium by incubating resected and cleaned trachea in radioimmunoprecipitation assay (RIPA) buffer with Complete Mini Protease Inhibitor Cocktail Tablet (Roche, #11836153001) for 30 min on ice. Western blot followed the standard protocols. Mouse anti-β-Actin (Sigma, #A5441, ∼46 KDa) was used as loading

Author Manuscript Author Manuscript Author Manuscript Author Manuscript

control at 1:40,000 dilution. Rabbit anti-Cp110 (Thermo scientific, # PA5-34380, ~120 KDa) was used at 1:1000 dilution in 5% non-fat dry milk in TBS-T (20mM Tris pH=7.6, 150mM NaCl and 0.1%Tween-20). Horseradish Peroxidase (HRP) conjugated secondary antibodies (Santa Cruz Biotechnology, #sc-2004 and #sc-2005) were used at 1:5000 dilution. Blots were analyzed using Image J. Band intensities were normalized against corresponding Actin and compared to WT controls for ratio calculation.

Manipulation of *Xenopus* Embryos and skin explants

X. laevis eggs were collected and *in vitro*-fertilized, then cultured and microinjected by standard procedures[46]. Embryos were injected with morpholino nucleotides (MOs, Gene Tools) at the two- to four-cell stage using a PicoSpritzer setup in 1/3× Modified Frog Ringer's solution (MR) with 2.5% Ficoll PM 400 (GE Healthcare 17-0300-50), and then were transferred into 1/3× MR containing Gentamycin[46] after injection. Drop size was calibrated to about 7–8 nL per injection. Rhodamine-B dextran (0.5–1.0 mg/mL; Invitrogen D1841) was coinjected and used as lineage tracer. MO (Gene tools) doses were administered as follows: a total dose of 30 ng *miR-34/449* MOs; 10 ng each for *miR-34a* MO (5′-CAACAACCAGCTAAGACACTGCCAA 3′), *miR-34b* MO (5′ACAATCAGCTAACTACACTGCCTGA 3′), and *miR-449a* MO (5′AACCAGCTAACATTACACTGCCTT 3′), or 30 ng of a miR-control MO (5′ TGCACGTTTCAATACAGACCGT 3′), or 17ng of *cp110* MO (5′-ACTCTTCATATGGCTCCATGGTCCC-3′). An mRNA encoding Centrin-4 RFP/GFP[37] and Sas6-GFP[29] was prepared using the Ambion message machine kit using sp6 (AM1340) and diluted to 50-100 ng/μL for injection into the embryos (0.8-1.6ng total/embryo). *Xenopus tropicalis cp110* cDNA (PureYield Midiprep; Promega, #A2495) was derived from a clone matching BC167469 obtained from Thermo Scientific (#MXT1765-202715711). *Cp110*Δ3′UTR was generated from the same clone, which was digested with Sph1 (New England Biolabs, #R0182S) and re-ligated to remove most of the 3′UTR. Analysis of morphant tadpole brains for signs of hydrocephalus was performed as previously described[50].

Xenopus skin explants were generated from animal caps[46], dissected in 1× Modified Barth's Saline from stage 9 embryos, which were either uninjected (time course experiment) or injected with Ctrl MO or *miR-34/449* MOs (for quantification of *cp110* and *foxj1* expression). Explants were cultured in 0.5×Modified Barth's Saline until unmanipulated control embryos reached appropriate stage. In the time course experiment, stage 10, 26 and 32 explants represented ciliation state of MCCs for quantitation of *cp110, foxj1, and miR-34/449* miRNAs. In addition, *cp110* and *foxj1* expression levels in Ctrl MO and *miR-34/449* MOs injected embryos (injected 4× into the animal hemisphere at the 4 cell stage) were assessed at onset of ciliation (stage 26 explants) to examine the effect of *miR-34/449* on *foxj1* and *cp110* levels. Statistical evaluation of experimental data was performed using chi-squared tests (http://www.physics.csbsju.edu/stats/contingency.html) or Wilcoxon sum of ranks (Mann-Whitney) tests (http://www.fon.hum.uva.nl/Service/Statistics/Wilcoxon_Test.html).

Author Manuscript Author Manuscript Author Manuscript Author Manuscript

Sample size and analysis

Sample sizes for all experiments were chosen based on previous experiences. No randomization or blinding was applied for all our studies.

Ethics statement on animal experiments

This work was done with approval of University of California, Berkeley's Animal Care and Use Committee. University of California, Berkeley's assurance number is A3084-01, and is on file at the National Institutes of Health Office of Laboratory Animal Welfare.

Extended Data

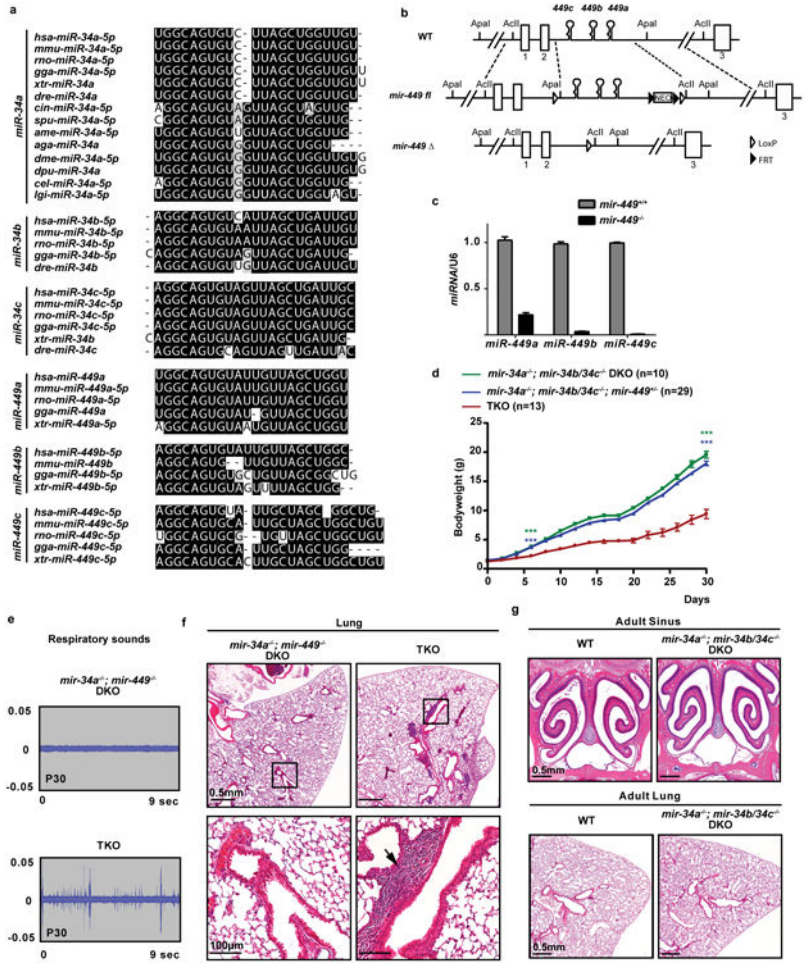

Extended Data Figure 1. The generation and phenotypic characterization of *miR-34/449* TKO mice

a. *miR-34/449* miRNAs are evolutionarily conserved with extensive sequence homology across many species. *miR-34a* has a more ancient evolutionary history compared to the rest of *miR-34/449* miRNAs. *miR-34a* is conserved in Deuterostome, Ecdysozoa and Lophotrochozoa, yet the rest of miR-*34/449* miRNAs have only vertebrate homologues. **b.** Diagrams of the targeted deletion strategy to generate *mir-449* knockout mice. Since all *mir-449* miRNAs are within intron 2 of their host gene, *cdc20b*, we deleted *mir-449* with a

Author Manuscript Author Manuscript Author Manuscript Author Manuscript

minimally predicted impact on *cdc20b*. **c.** *miR-449* expression is absent in *mir-449*$^{-/-}$ knockout animals, as demonstrated by real time PCR analyses in lung tissues from littermate-controlled wild-type and *mir-449*$^{-/-}$ mice at postnatal day 35. n=3. *miR-449a* real time PCR primers exhibit a modest cross-reaction with *miR-34* miRNAs. **d.** *miR-34/449* TKO mice have a significant postnatal attenuation in body weight. Littermate-controlled *mir-34a*$^{-/-}$; *mir-34b/34c*$^{-/-}$, *mir-34a*$^{-/-}$; *mir-34b/34c*$^{-/-}$; *mir-449*$^{+/-}$ and TKO mice were monitored for their body weight every other day for 30 days after birth. Paired *t*-test, *** $P<0.001$. **e**. Surviving *miR-34/449* TKO mice exhibit coughing/sneezing-like phenotype. The respiratory noise of littermate-controlled *mir-34a*$^{-/-}$; *mir-449*$^{-/-}$ DKO and TKO mice was shown by sound wave analysis at postnatal day 30. n=14. **f.** Pulmonary inflammation occurs in a subset of *miR-34/449* TKO mice. A representative H&E analysis of lung tissues from an adult TKO mouse indicates an increased infiltration by inflammatory cells. 3 out of 15 TKO mice examined exhibit lung infection. **g**. *mir-34a*$^{-/-}$; *mir-34b/34c*$^{-/-}$ DKO mice resemble wild-type mice, exhibiting no obvious respiratory defects in paranasal sinus or lung. n=3. All error bars represent s.e.m.

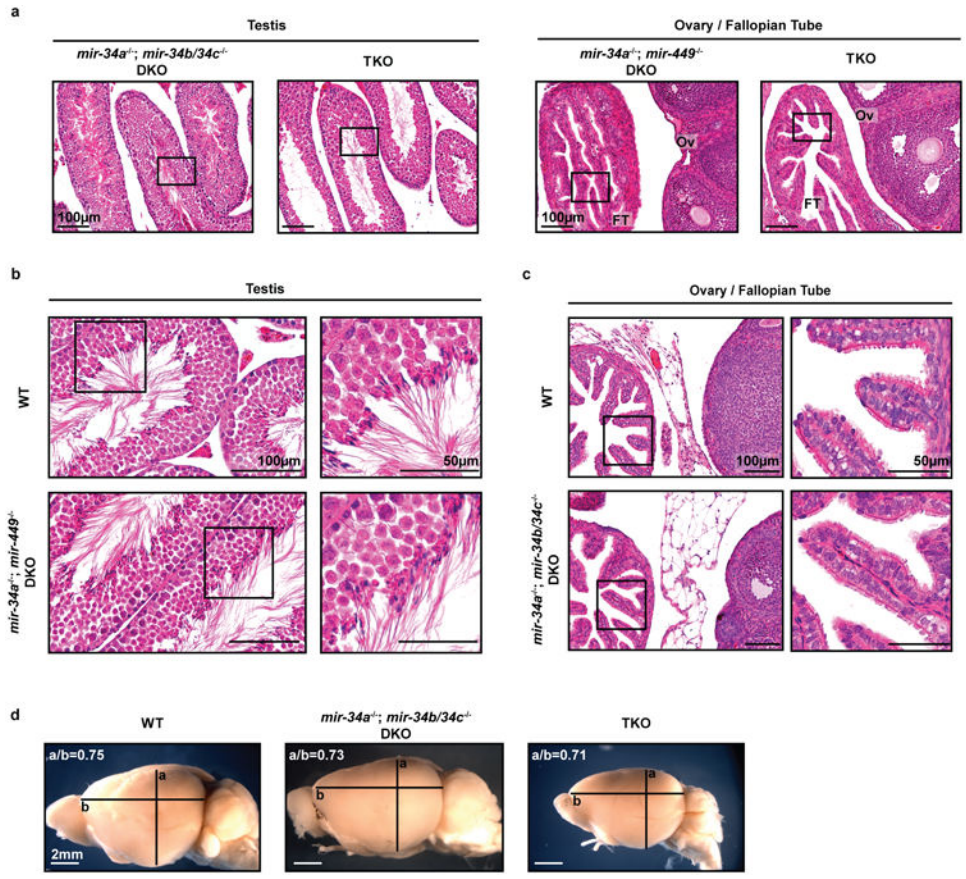

Extended Data Figure 2. Phenotypic characterization of reproductive organs and brain in *miR-34/449* TKO mice

a. Adult male and female *miR-34/449* TKO mice are infertile. Male (left) and female (right) reproductive organs from littermate-controlled DKO and TKO mice were subjected to H&E staining. n=3. Boxes indicate areas depicted in Figure 1e. **b.** Adult *mir-34a*$^{-/-}$; *mir-449*$^{-/-}$

Author Manuscript Author Manuscript Author Manuscript Author Manuscript

DKO male mice exhibit no defects in spermatogenesis. **c.** Adult *mir-34a*$^{-/-}$; *mir-34b/34c*$^{-/-}$ DKO female mice display no defects in reproductive organs. **d**. The adult *mir-34/449* TKO brains do not exhibit hydrocephalus, yet they are smaller in size than wild-type and DKO controls. a/b: the coronal to horizontal ratios. n=3 for **b**, **c** and **d**.

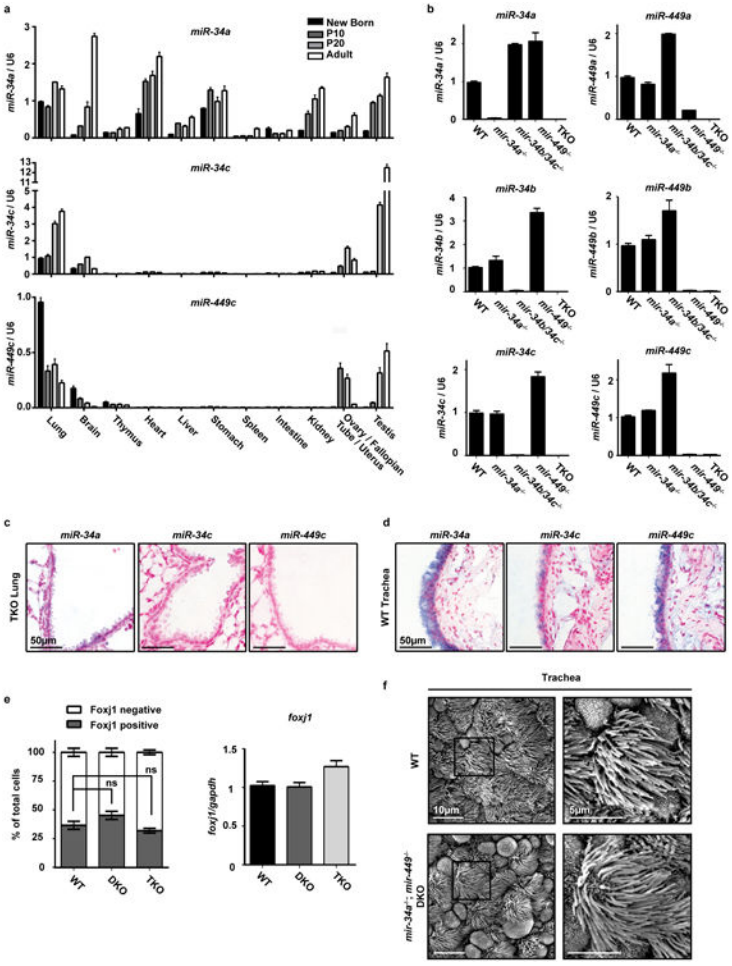

Extended Data Figure 3. *miR-34/449* miRNAs are enriched in airway MCCs

a. Most *miR-34/449* miRNAs are enriched in tissues with motile cilia. Using real time PCR, the expression of *miR-34a*, *miR-34c*, and *miR-449c* were measured in multiple tissues from newborn, P10, P20, and adult wild-type mice. Both *miR-34c* and *miR-449c* are exclusively expressed in tissues with motile cilia, while *miR-34a* exhibits a broader expression pattern. n=3. **b.** The real time PCR assay for each *miR-34/449* miRNA specifically detects the corresponding miRNA. The specificity of each miRNA real time PCR assay was validated using testis RNA from wild-type (WT), *mir-34a*$^{-/-}$, *mir-34b/34c*$^{-/-}$, *mir-449*$^{-/-}$, and TKO mice at postnatal day 35. The *miR-449a* assay shows a slight cross reaction with homologous miRNAs. n=3. **c.** *In situ* hybridization of each *miR-34/449* miRNA exhibits specific detection. No measurable *miR-34/449 in situ* signal is detected in TKO lung sections at postnatal day 25. n=2. **d.** *miR-34/449* miRNAs are enriched in tracheal MCCs. *In situ* hybridization analyses demonstrate that *miR-34c* and *miR-449c* are specifically expressed in the tracheal MCCs, while *miR-34a* is expressed in both tracheal MCCs and the surrounding

Author Manuscript Author Manuscript Author Manuscript Author Manuscript

cell types. n=2. **e**. *miR-34/449* TKO mice do not exhibit significant alterations in Foxj1 expression. Quantification of Foxj1 positive cells (left, n=3) and *foxj1* mRNA (right, n=4) was performed for well controlled wild-type, DKO and TKO tracheas, using immunofluorescence and real time PCR, respectively. Paired *t*-test, ns: $P > 0.05$. **f**. *mir-34a*$^{-/-}$; *mir-449*$^{-/-}$ DKO tracheal epithelia are morphologically indistinguishable from wild-type controls in scanning electron microscopy (SEM) analyses. n=3. All error bars represent s.e.m.

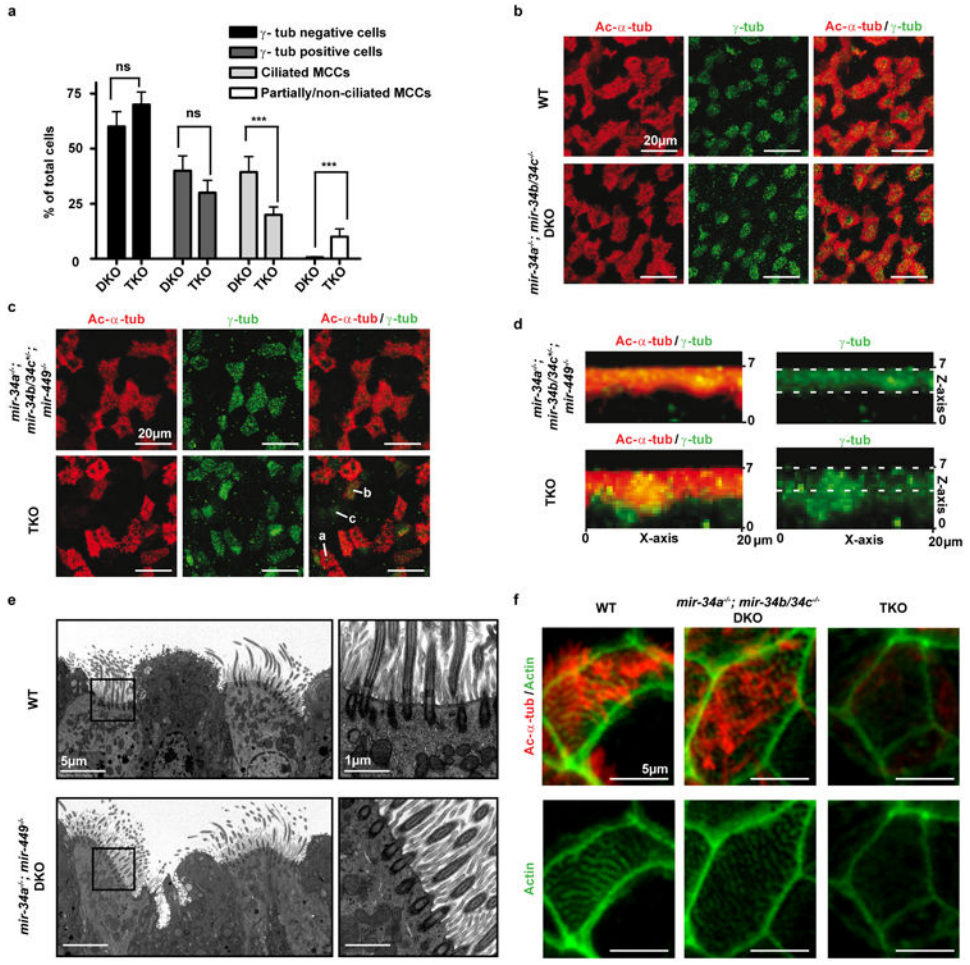

Extended Data Figure 4. *miR-34/449* deficiency causes defective ciliation and basal body docking in mouse airway MCCs

a. *miR-34/449* TKO trachea exhibit reduced MCC ciliation. Quantification of fully ciliated MCCs (γ-tub and Ac-α-tub double-positive) and partially/non-ciliated MCCs, Ac-α-tub weak/negative) was performed in littermate controlled DKO and TKO mouse tracheas, using data from all three experiments in Figure 3a. The number of cells with MCC identity (γ-tub positive) is unaffected in TKO tracheas, yet one third of the TKO MCCs display aberrant Ac-α-tub staining, indicating ciliation defects. Paired *t*-test, ns: $P > 0.05$, *** $P < 0.001$. **b.** The *mir-34a*$^{-/-}$; *mir-34b/34c*$^{-/-}$ DKO mice exhibit normal ciliogenesis in tracheal MCCs. Whole tracheas from age matched adult wild-type and *mir-34a*$^{-/-}$; *mir-34b/34c*$^{-/-}$ DKO mice were analyzed by immunofluorescence staining for Ac-α-tub (cilia) and γ-

Author Manuscript Author Manuscript Author Manuscript Author Manuscript

tubulin (basal bodies). n=3 **c.** *miR-34/449* TKO primary tracheal epithelial cells exhibit ciliation defects in air liquid interface (ALI) culture. ALI culture of MCCs were derived from tracheas of littermate-controlled *mir-34a*$^{-/-}$; *mir-34b/34c*$^{+/-}$; *mir-449*$^{-/-}$ and TKO mice, and subjected to immunofluorescence staining for Ac-α-tub (cilia) and γ-tub (basal bodies). In TKO and control ALI culture, comparable levels of γ-tub positive cells are observed, yet a large portion of TKO γ-tub positive cells displayed a partial or complete loss of Ac-α-tub staining. a: fully, b: partially, c: non ciliated MCCs; n=2. **d**. Basal bodies fail to dock to the apical membrane of *miR-34/449* TKO MCCs in ALI culture. Lateral projections of confocal micrographs described in (**c**) show impaired apical localization of γ-tub staining in TKO MCCs from ALI cultures, suggesting a defective basal body docking to the apical membrane. **e**. *mir-34a*$^{-/-}$; *mir-449*$^{-/-}$ DKO trachea exhibit no defects in basal body docking using transmission electron microscopy (TEM) analyses. n=3. **f**. TKO tracheal MCCs exhibit a defective subapical Actin network. Whole tracheas from adult wild-type, *mir-34a*$^{-/-}$; *mir-34b/34c*$^{-/-}$ DKO and TKO mice were analyzed by immunofluorescence staining for Ac-α-tub (cilia) and phalloidin-488 (Actin). n=2. All error bars represent s.e.m.

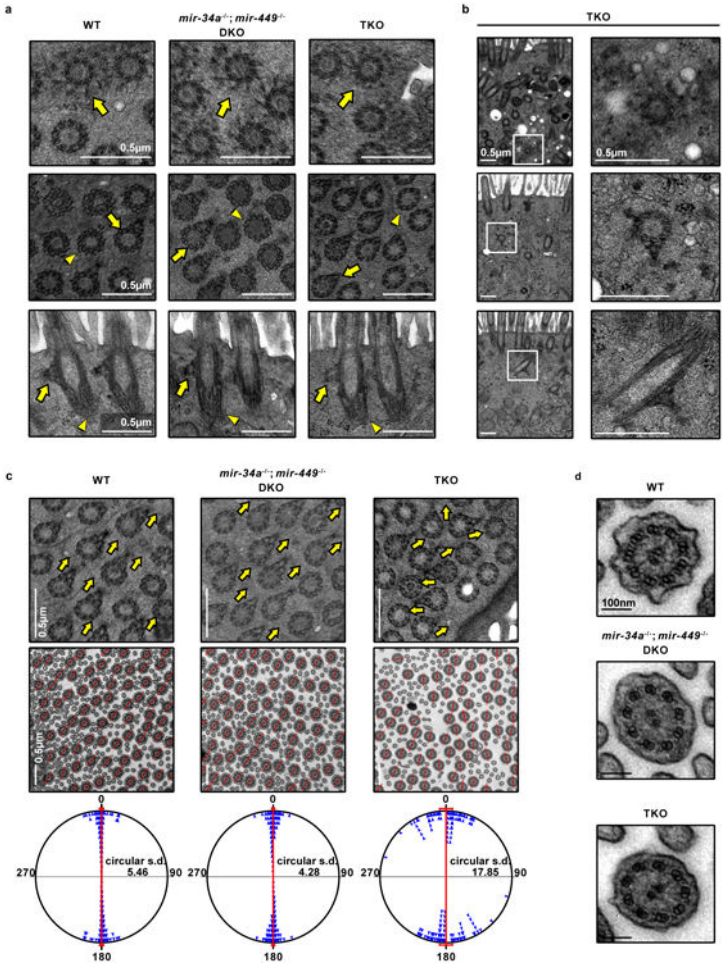

Extended Data Figure 5. Major basal body structural components are intact in *miR-34/449* TKO MCCs revealed by transmission electron microscopy

Author Manuscript Author Manuscript Author Manuscript Author Manuscript

Apically docked (**a**) and undocked (**b**) basal bodies in *miR-34/449* TKO MCCs have intact structural components. Basal body transition fibers (top), basal feet (middle) and striated rootlets (bottom) have comparable morphology among WT, DKO and TKO MCCs. Top panel: arrow, a representative transverse view of transition fibers. Middle panel: arrow, a representative transverse view of nine microtubule triplets with basal feet; arrowhead, a representative transverse view collected from a different height of a basal body, containing nine microtubule triplets without basal feet. Bottom panel: arrow, the longitudinal view of basal feet; arrowhead, the striated rootlet structure. **c**. Directionality of basal bodies (top) and axonemes (middle) is moderately affected in *miR-34/449* TKO MCCs. Top panel: arrows point to the directions indicated by basal foot. Middle panel: red lines connecting the central pair of axonemes indicate the rotational polarity of each ciliary axoneme. Bottom panel: the angles of the axoneme directionality were statistically analyzed as bidirectional circular data. The average angel was set from 0° to 180° axis. *miR-34/449* TKO ciliary axonemes have moderately un-coordinated directionality compared to WT and DKO controls. **d**. *miR-34/449* TKO axonemes exhibit intact structures, including nine outer microtubule doublets, two central microtubule singlets, and dynein arms. n=3.

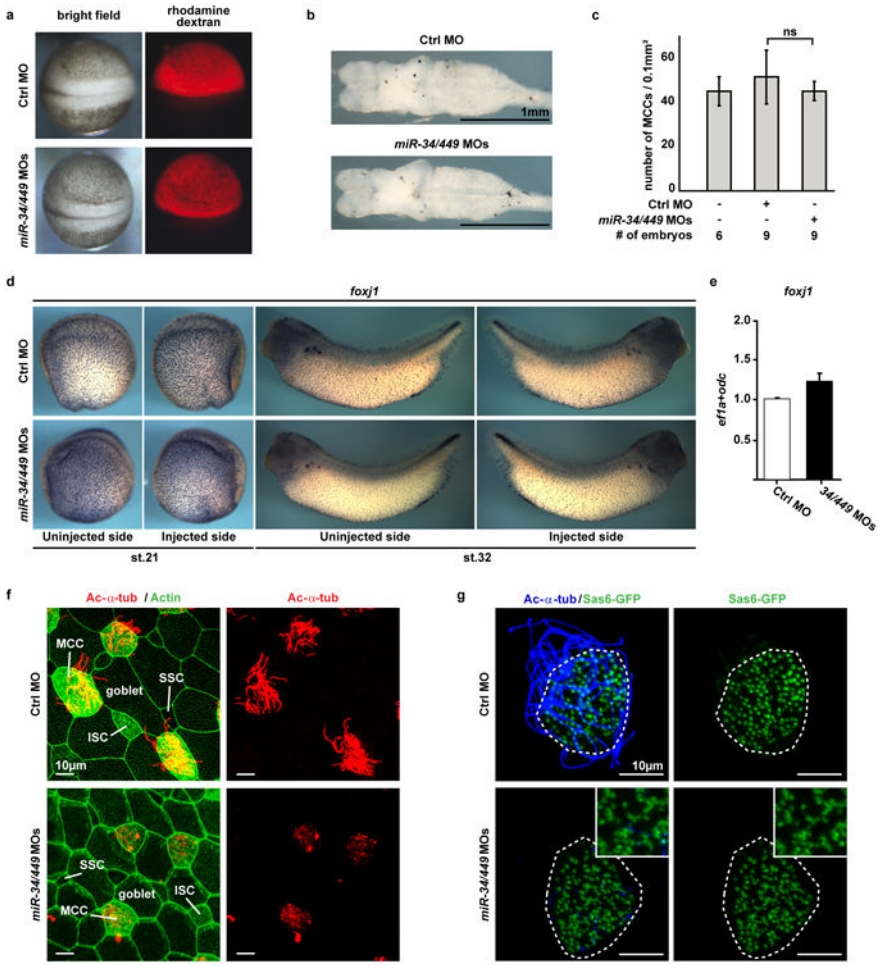

Extended Data Figure 6. *miR-34/449* deficiency in frog MCCs causes defective ciliogenesis without affecting cell fate specification

Author Manuscript Author Manuscript Author Manuscript Author Manuscript

a. Injection of Ctrl or *miR-34/449* MOs does not affect general embryonic development or neural tube closure. *Xenopus laevis* embryos were injected unilaterally with MOs at the 2-4 cell stage and analyzed at neurula stages (18-20). Targeting of the skin ectoderm was confirmed by coinjection of fluorescent rhodamine dextran. **b.** Frog *miR-34/449* morphants do not exhibit hydrocephalus. Embryos were injected animally with control or *miR-34/449* MOs into both dorsal blastomeres at the 4 cell stage to target the neural tube and brain regions. Subsequently, the whole brains were dissected and analyzed at stage 45/46. The lack of hydrocephalus in *miR-34/449* morphants argues against a role of *miR-34/449* in ependymal ciliation. **c.** Quantification of fully ciliated, partially ciliated or non-ciliated MCCs reveals no significant change in total number of MCC-fated cells in *miR-34/449* morphants. Error bars represent s.d. Wilcoxon Two Sample test, n.s., $P > 0.05$. **d, e.** *foxj1* expression and specification of MCC fate is unaltered in *miR-34/449* deficient embryos. **d.** Embryos were unilaterally injected with Ctrl or *miR-34/449* MOs to the right side at 2-4 cell stage, cultured until stage 21 or 32 and processed for *in situ* hybridization to monitor *foxj1* expression in the mucociliary epithelium of the skin. No change in *foxj1* expression can be detected. **e.** Real time PCR analysis in Ctrl or *miR34/449* MOs injected skin explants at stage 26 (onset of ciliation) does not indicate reduced expression levels of *foxj1*. **f.** *miR-34/449* deficient frog embryos exhibit normal development of the mucociliary ectodermal epithelium. Detailed analysis of the embryonic skin at stage 30-32 reveals the presence (specification and intercalation) of all cell types in *miR-34/449* morphants, including large goblet cells, small secretory cells (SSC), Ac-α-tub positive ciliated cells (MCC) and non-tubulin enriched ion secreting cells (ISC). **g.** *miR-34/449* morphant MCCs exhibit an uneven distribution of basal bodies. *Sas6-gfp* mRNA was injected at the 2-4 cell stage to visualize basal bodies at stage 30-32. In control embryos Sas6-GFP foci are evenly distributed in fully ciliated MCCs, while *miR-34/449* morphant MCCs are characterized by an uneven distribution and aggregation of basal bodies, which frequently fail to grow cilia (Ac-α-tub staining). Such phenotype is characteristic for basal body docking defects. Embryos/cells analyzed: Ctrl MO (4/7), *miR-34/440*MOs (6/10).

Author Manuscript Author Manuscript Author Manuscript Author Manuscript

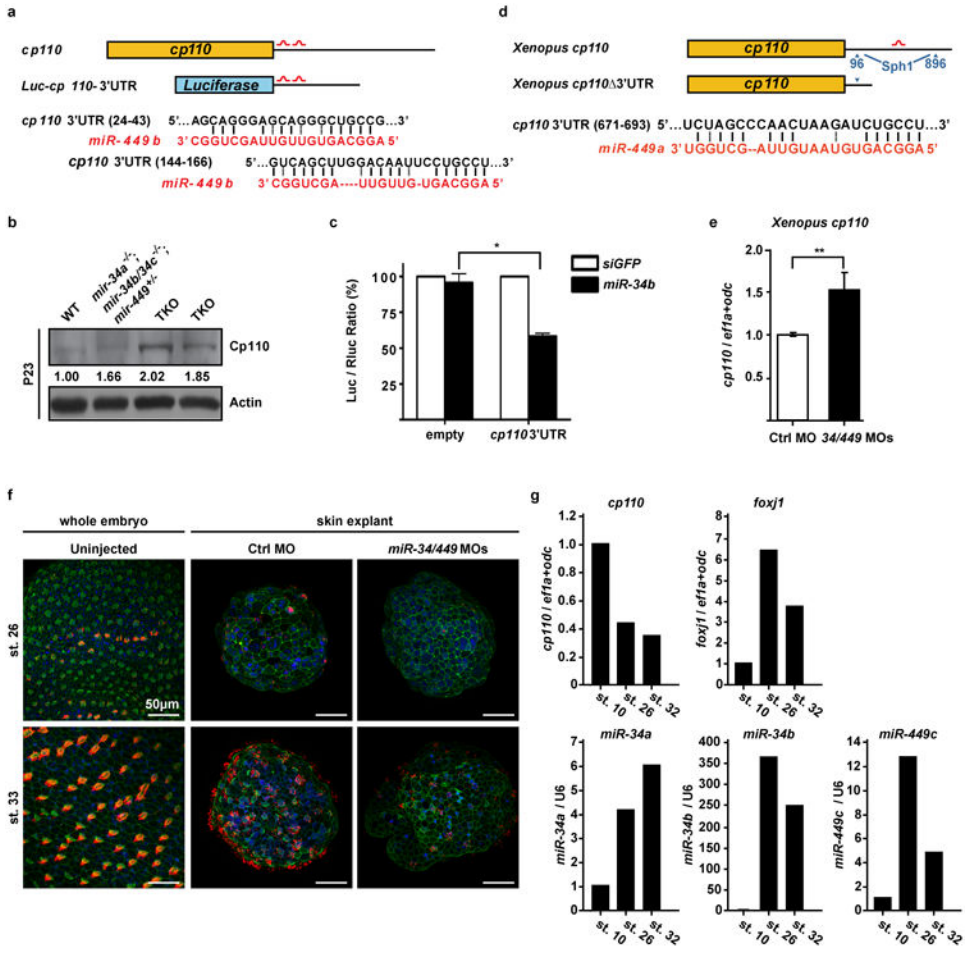

Extended Data Figure 7. *cp110* is a direct target of *miR-34/449* miRNAs

a. A schematic representation of two predicted *miR-34/449* binding sites in the mouse c*p110* 3′UTR and in the luciferase reporter construct that contains *cp110* 3′UTR. **b.** Cp110 protein levels at postnatal day 23 are elevated in *miR-34/449* TKO tracheal epithelia. **c.** The expression of *Luc-cp110-3′UTR* exhibits *miR-34b*-dependent repression in NIH/3T3 cells. Error bars represent s.e.m., n=3. Paired *t*-test, * $P < 0.05$. **d.** A schematic representation of one predicted *miR-34/449* binding site in the frog c*p110* 3′UTR. A truncated *cp110* construct, *cp110*Δ3′UTR, was made to generate a *cp110* cDNA without the *miR-34/449* target site. **e.** Real time PCR monitoring *cp110* reveals elevated mRNA expression levels of *cp110* in *miR-34/440* morphant frog skin explants as compared to Ctrl MO injected specimens. **f.** Timeline of MCC ciliation and recapitulation of ciliation defects in skin explants (animal caps). Representative confocal images from staged whole embryos and skin explants injected with either Ctrl MO or *miR-34/449* MOs show the onset of ciliation at stage 26 and fully ciliated skin ectoderm at stage 32 in whole embryos and Ctrl MO injected skin explants. *miR-34/449* MOs injected skin explants develop MCC ciliogenesis defects comparable to whole embryo treatment. Cilia: Ac-α-Tub (red), Actin: Phalloidin-488 (green) and nuclei: DAPI (blue). **g.** Expression of *cp110*, *foxj1* and *miR-34/449* RNAs during time course of ciliation in skin explants. Explants at stage 10 represent unciliated MCC precursors, explants at stage 26 represent MCCs at the onset of ciliation, and stage 32

Author Manuscript Author Manuscript Author Manuscript Author Manuscript

explants represent fully ciliated ectodermal epithelium. *cp110* mRNA levels decrease over the time course of ciliation, with the strongest decrease between stage 10 and 26, while *foxj1* mRNA levels rapidly increase during this time. *miR-34a*, *-34b* and *-449c* levels strongly increase between stage 10 and stage 26; and only a moderate increase or even decrease can be observed between stage 26 and 32, similar to *foxj1* expression levels. Error bars represent s.e.m. n=2, technical replicates on pools of 30 skin explants for each time point.

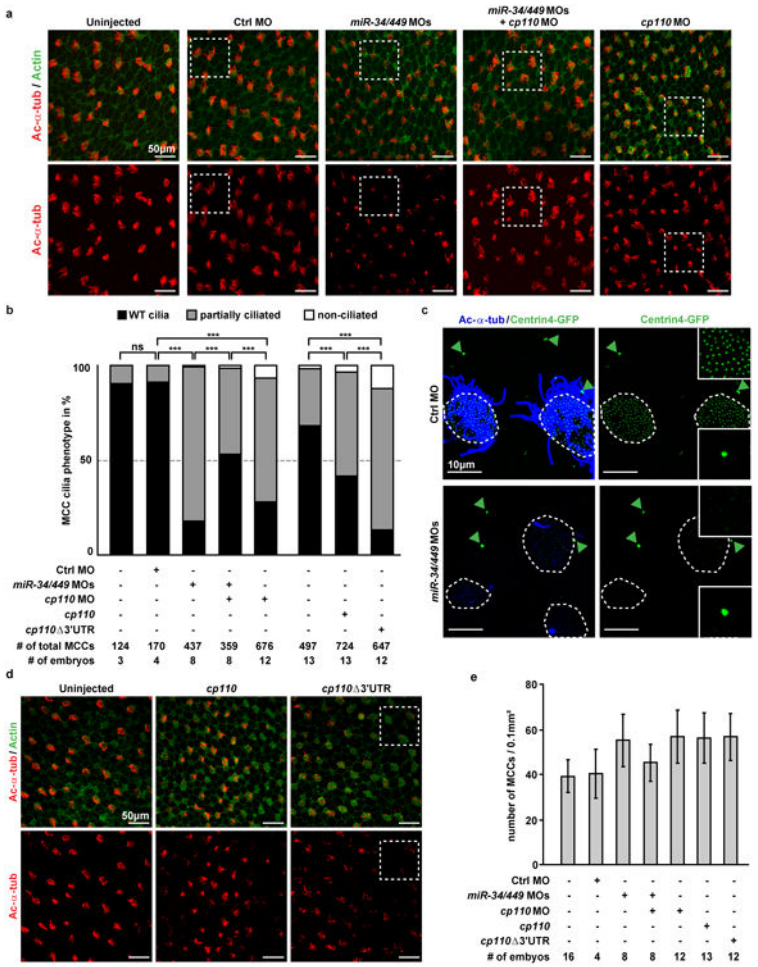

Extended Data Figure 8. *miR-34/449* miRNAs promote ciliogenesis by repressing *cp110*

a. Representative examples of confocal images used for quantification of MCC ciliation in (**b**). Embryos were stained for Ac-α-tub (cilia) and phalloidin-488 (Actin). White boxes indicate areas depicted in Figure 5c. **b.** Quantification of MCC ciliation in (**a**), (**d**) and Figure 5c. χ^2-test, ns $P > 0.05$, *** $P < 0.001$. **c.** Centrin4-GFP incorporation into basal bodies is affected in *miR-34/449* deficient embryos. *centrin4-gfp* mRNA was injected at 2-4 cell stage to visualize basal bodies in MCCs at stage 32, and centrosomes in neighboring epithelial cells. In Ctrl morphant embryos, Centrin4-GFP staining in basal bodies (smaller foci in ciliated cells) and centrosomes (bigger foci in non-ciliated cells, green arrowheads) are equally strong. In contrast, Centrin4-GFP staining in basal bodies is greatly reduced in *miR-34/449* morphants, without alteration of fluorescent intensity in centrosomes of neighboring cells. Embryos/cells analyzed: Ctrl MO (6/17), *miR-34/449* MOs (7/23). **d.**

Author Manuscript Author Manuscript Author Manuscript Author Manuscript

Representative examples of confocal images from *cp110* overexpression experiments used for quantification of MCC ciliation in (**b**). White boxes indicate areas depicted in Figure 5c. **e.** The number of MCC-fated cells in *miR-34/449* or *cp110* morphants, and embryos injected with *cp110* DNA constructs is not reduced. Quantification of total MCC numbers (fully ciliated, partially ciliated or non-ciliated MCCs) is shown for frog embryos injected with various MOs/DNAs (corresponding to (**a**), (**b**), (**d**) and Figure 5c). Error bars represent s.d.

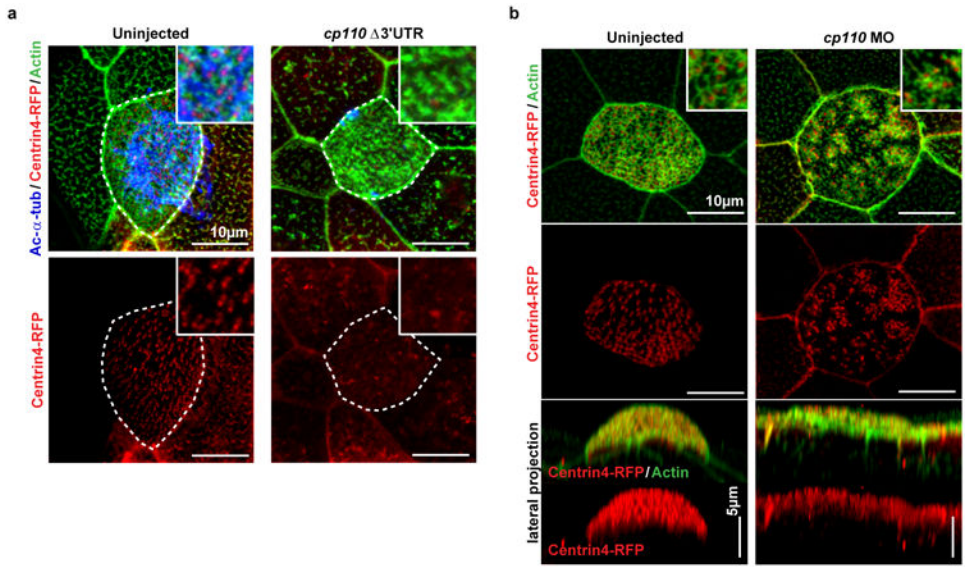

Extended Data Figure 9. Gain and loss of *cp110* affects MCC basal bodies, but not the subapical Actin meshwork

a. *cp110* overexpression phenocopies *miR-34/449* knockdown. Centrin4-RFP enrichment is strongly reduced in *cp110*Δ3′UTR overexpressing MCCs. It is noteworthy, that while ciliation and incorporation of Centrin4 are strongly affected in *cp110*Δ3′UTR injected embryos, formation of the subapical Actin meshwork appears largely unaffected. Together with the lack of *cp110* knockdown to rescue the subapical Actin meshwork in *miR-34/449* morphants, these data indicate an additional effect of *miR-34/449* miRNAs on Actin formation/organization, which is *cp110* independent. Cilia: Ac-α-tub, basal bodies: Centrin4-RFP, Actin: phalloidin-488. Embryos/cells analyzed: Uninjected (4/7), *cp110*Δ3′URT (6/10). **b.** The cellular basis for ciliation defects in *cp110* morphants is likely due to the atypical failure of basal bodies to separate from each other, thus they appear to be aggreageted in clusters of *cp110*-deficient MCCs. Nevertheless, Centrin4 incorporation or apical localization of basal bodies is not affected in *cp110* morphants. Basal bodies: Centrin4-RFP, Actin: phalloidin-488. Embryos/cells analyzed: Uninjected (2/3), cp110 MO (5/8). Embryos were derived from at least two females and independent fertilizations per *Xenopus* experiment.

Author Manuscript Author Manuscript Author Manuscript Author Manuscript

Extended Data Table 1

Candidate *miR-34/449* targets with potential roles in MCC differentiation and/or ciliation in respiratory epithelia.

Gene Symbol	Gene Name
Ank3	ankyrin 3, epithelial
Atp2b4	ATPase, Ca++ transporting, plasma membrane 4
Aurka	aurora kinase A
Aurkb	aurora kinase B
Ccdc39	coiled-coil domain containing 39
Ccdc40	coiled-coil domain containing 40
Ccna2	cyclin A2
Ccnb1	cyclin B1
Ccnd2	cyclin D2
Ccne2	cyclin E2
Ccp110	centriolar coiled coil protein 110
Cdc25a	cell division cycle 25A
Cdc6	cell division cycle 6
Cdca7l	cell division cycle associated 7 like
Cdk5rap2	CDK5 regulatory subunit associated protein 2
Cep152	centrosomal protein 152
Cep63	centrosomal protein 63
Cep97	centrosomal protein 97
Chek1	checkpoint kinase 1
Daam1	dishevelled associated activator of morphogenesis 1
Dnah5	dynein, axonemal, heavy chain 5
Dnali1	dynein, axonemal, light intermediate polypeptide 1
Dtl	denticleless homolog (Drosophila)
Dzip1	DAZ interacting protein 1
Fat4	FAT tumor suppressor homolog 4 (Drosophila)
Fgfr1	fibroblast growth factor receptor
Foxg1	forkhead box G1
Foxj1	forkhead box J1
Hdac6	histone deacetylase 6
Hook3	hook homolog 3 (Drosophila)
lft27	intraflagellar transport 27
Itch	itchy, E3 ubiquitin protein ligase
Jag1	jagged 1
Kif24	kinesin family member 24
Lef1	lymphoid enhancer binding factor 1
Mapt	microtubule-associated protein tau
Met	met proto-oncogene
Myb	myeloblastosis oncogene

Author Manuscript Author Manuscript Author Manuscript Author Manuscript

Gene Symbol	Gene Name
Myh9	myosin, heavy polypeptide 9, non-muscle
Pacs1	phosphofurin acidic cluster sorting protein 1
Pdgfra	platelet derived growth factor receptor, alpha polypeptide
Pofut1	protein O-fucosyltransferase 1
Rdh11	retinol dehydrogenase 11
Rfx3	regulatory factor X, 3
Rrm2	ribonucleotide reductase M2
Shank3	SH3/ankyrin domain gene 3
Six3	sine oculis-related homeobox 3
Skp2	S-phase kinase-associated protein 2 (p45)
Stat6	signal transducer and activator of transcription 6
Stil	Scl/Tal1 interrupting locus
Stk36	serine/threonine kinase 36
Tmem107	transmembrane protein 107
Tppp	tubulin polymerization promoting protein
Tsc2	tuberous sclerosis 2
Ttc26	tetratricopeptide repeat domain 26
Ttll3	tubulin tyrosine ligase-like family, member 3
Xpnpep3	X-prolyl aminopeptidase (aminopeptidase P) 3, putative

Supplementary Material

Refer to Web version on PubMed Central for supplementary material.

Acknowledgments

We thank MJ Bennett, M Butler, B Dynlacht, W Finkbeiner, P Kysar, B Lee, T Machen, B Mitchell, and J Wallingford for constructs, technical assistance, stimulating discussions and helpful input. We also thank P Margolis for careful reading of our manuscript. LH acknowledges an R01 and an R21 grant from NCI (R01 CA139067, 1R21CA175560-01), a CIRM new faculty award (RN2-00923-1), a TRDRP research grant (21RT-0133), and a research scholar award from American Cancer Society (ACS, 123339-RSG-12-265-01-RMC). RS acknowledges the support of Siebel postdoctoral fellowship and CIRM postdoctoral fellowship. PW was funded by the Deutsche Forschungsgemeinschaft (DFG, Wa 3365/1-1), and frog work in the Harland laboratory was funded by NIH grant GM42341. ML would like to thank M. Dobbelstein for support and discussions, and was financed by a Dorothea Schloezer Fellowship.

References

1. Ambros V. The functions of animal microRNAs. Nature. 2004; 431:350–355. [PubMed: 15372042]
2. He L, Hannon GJ. MicroRNAs: small RNAs with a big role in gene regulation. Nat Rev Genet. 2004; 5:522–31. [PubMed: 15211354]
3. Kim VN. Small RNAs: classification, biogenesis, and function. Mol Cells. 2005; 19:1–15. [PubMed: 15750334]
4. Du T, Zamore PD. microPrimer: the biogenesis and function of microRNA. Development. 2005; 132:4645–4652. [PubMed: 16224044]
5. Lee RC, Feinbaum RL, Ambros V. The C. elegans heterochronic gene lin-4 encodes small RNAs with antisense complementarity to lin-14. Cell. 1993; 75:843–54. [PubMed: 8252621]

Author Manuscript Author Manuscript Author Manuscript Author Manuscript

6. Wightman B, Ha I, Ruvkun G. Posttranscriptional regulation of the heterochronic gene lin-14 by lin-4 mediates temporal pattern formation in C. elegans. Cell. 1993; 75:855–862. [PubMed: 8252622]
7. Miska EA, et al. Most Caenorhabditis elegans microRNAs are individually not essential for development or viability. PLoS Genet. 2007; 3:e215. [PubMed: 18085825]
8. Park CY, et al. A Resource for the Conditional Ablation of microRNAs in the Mouse. Cell Rep. 2012; 1:385–391. [PubMed: 22570807]
9. Marson A, et al. Connecting microRNA Genes to the Core Transcriptional Regulatory Circuitry of Embryonic Stem Cells. Cell. 2008; 134:521–533. [PubMed: 18692474]
10. Marcet B, et al. Control of vertebrate multiciliogenesis by miR-449 through direct repression of the Delta/Notch pathway. Nat Cell Biol. 2011; 13:694–701.
11. He L, et al. A microRNA component of the p53 tumour suppressor network. Nature. 2007; 447:1130–4. [PubMed: 17554337]
12. Chang TC, et al. Transactivation of miR-34a by p53 broadly influences gene expression and promotes apoptosis. Mol Cell. 2007; 26:745–52. [PubMed: 17540599]
13. Raver-Shapira N, et al. Transcriptional activation of miR-34a contributes to p53-mediated apoptosis. Mol Cell. 2007; 26:731–743. [PubMed: 17540598]
14. He L, He X, Lowe SW, Hannon GJ. microRNAs join the p53 network--another piece in the tumour-suppression puzzle. Nat Rev Cancer. 2007; 7:819–822. [PubMed: 17914404]
15. Hermeking H. p53 enters the microRNA world. Cancer Cell. 2007; 12:414–418. [PubMed: 17996645]
16. Satir P, Christensen ST. Overview of structure and function of mammalian cilia. Annu Rev Physiol. 2007; 69:377–400. [PubMed: 17009929]
17. Fliegauf M, Benzing T, Omran H. When cilia go bad: cilia defects and ciliopathies. Nat Rev Mol Cell Biol. 2007; 8:880–893. [PubMed: 17955020]
18. Spektor A, Tsang WY, Khoo D, Dynlacht BD. Cep97 and CP110 suppress a cilia assembly program. Cell. 2007; 130:678–90. [PubMed: 17719545]
19. Tsang WY, Dynlacht BD. CP110 and its network of partners coordinately regulate cilia assembly. Cilia. 2013; 2:9. [PubMed: 24053599]
20. Choi YJ, et al. miR-34 miRNAs provide a barrier for somatic cell reprogramming. Nat Cell Biol. 2011; 13:1353–1360. [PubMed: 22020437]
21. Lizé M, Klimke A, Dobbelstein M. MicroRNA-449 in cell fate determination. Cell Cycle. 2011; 10:2874–2882. [PubMed: 21857159]
22. Loges NT, et al. DNAI2 mutations cause primary ciliary dyskinesia with defects in the outer dynein arm. Am J Hum Genet. 2008; 83:547–558. [PubMed: 18950741]
23. Castleman VH, et al. Mutations in radial spoke head protein genes RSPH9 and RSPH4A cause primary ciliary dyskinesia with central-microtubular-pair abnormalities. Am J Hum Genet. 2009; 84:197–209. [PubMed: 19200523]
24. Stubbs JL, Oishi I, Izpisúa Belmonte JC, Kintner C, Izpisu JC. The forkhead protein Foxj1 specifies node-like cilia in Xenopus and zebrafish embryos. Nat Genet. 2008; 40:1454–60. [PubMed: 19011629]
25. Marshall WF. Basal Bodies: Platforms for Building Cilia. Curr Top Dev Biol. 2008; 85:1–22. [PubMed: 19147000]
26. Avasthi P, Marshall WF. Stages of ciliogenesis and regulation of ciliary length. Differentiation. 2012; 83:S30–42. [PubMed: 22178116]
27. Werner ME, Mitchell BJ. Understanding ciliated epithelia: the power of Xenopus. Genesis. 2012; 50:176–85. [PubMed: 22083727]
28. Gomperts BN, Gong-Cooper X, Hackett BP. Foxj1 regulates basal body anchoring to the cytoskeleton of ciliated pulmonary epithelial cells. J Cell Sci. 2004; 117:1329–37. [PubMed: 14996907]
29. KlosDehring D, et al. Deuterosome-Mediated Centriole Biogenesis. Dev Cell. 2013; 27:103–112. [PubMed: 24075808]

Author Manuscript Author Manuscript Author Manuscript Author Manuscript

30. Martinez-Anton A, et al. Changes in microRNA and mRNA expression with differentiation of human bronchial epithelial cells. Am J Respir Cell Mol Biol. 2013; 49:384–95. [PubMed: 23590309]
31. Lewis BP, Burge CB, Bartel DP. Conserved seed pairing, often flanked by adenosines, indicates that thousands of human genes are microRNA targets. Cell. 2005; 120:15–20. [PubMed: 15652477]
32. Miranda KC, et al. A pattern-based method for the identification of MicroRNA binding sites and their corresponding heteroduplexes. Cell. 2006; 126:1203–1217. [PubMed: 16990141]
33. Hoh RA, Stowe TR, Turk E, Stearns T. Transcriptional program of ciliated epithelial cells reveals new cilium and centrosome components and links to human disease. PLoS One. 2012; 7:e52166. [PubMed: 23300604]
34. Tanos B, Yang H, Soni R. Centriole distal appendages promote membrane docking, leading to cilia initiation. Genes Dev. 2013; 27:163–168. [PubMed: 23348840]
35. Lai Y, et al. Inflammation-mediated upregulation of centrosomal protein 110, a negative modulator of ciliogenesis, in patients with chronic rhinosinusitis. J Allergy Clin Immunol. 2011; 128:1207–1215.e1. [PubMed: 21982113]
36. Cao J, et al. miR-129-3p controls cilia assembly by regulating CP110 and actin dynamics. Nat Cell Biol. 2012; 14:697–706. [PubMed: 22684256]
37. Park TJ, Mitchell BJ, Abitua PB, Kintner C, Wallingford JB. Dishevelled controls apical docking and planar polarization of basal bodies in ciliated epithelial cells. Nat Genet. 2008; 40:871–879. [PubMed: 18552847]
38. Delaval B, Covassin L, Lawson ND, Doxsey S. Centrin depletion causes cyst formation and other ciliopathy-related phenotypes in zebrafish. Cell Cycle. 2011; 10:3964–3972. [PubMed: 22142866]
39. Okada N, et al. A positive feedback between p53 and miR-34 miRNAs mediates tumor suppression. Genes Dev. 201410.1101/gad.233585.113
40. Kott E, et al. Loss-of-function mutations in RSPH1 Cause primary ciliary dyskinesia with central-complex and radial-spoke defects. Am J Hum Genet. 2013; 93:561–570. [PubMed: 23993197]
41. Kunimoto K, et al. Coordinated ciliary beating requires Odf2-mediated polarization of basal bodies via basal feet. Cell. 2012; 148:189–200. [PubMed: 22265411]
42. Deblandre GA, Wettstein DA, Koyano-Nakagawa N, Kintner C. A two-step mechanism generates the spacing pattern of the ciliated cells in the skin of Xenopus embryos. Development. 1999; 126:4715–28. [PubMed: 10518489]
43. Tsao PN, et al. Notch signaling controls the balance of ciliated and secretory cell fates in developing airways. Development. 2009; 136:2297–307. [PubMed: 19502490]
44. D'Angiolella V, et al. SCF(Cyclin F) controls centrosome homeostasis and mitotic fidelity through CP110 degradation. Nature. 2010; 466:138–142. [PubMed: 20596027]
45. Li J, et al. USP33 regulates centrosome biogenesis via deubiquitination of the centriolar protein CP110. Nature. 2013; 495:255–9. [PubMed: 23486064]
46. Sive HL, Grainger RM, Harland RM. Early Development of Xenopus laevis. 200010.1101/pdb.prot5536
47. Walentek P, Beyer T, Thumberger T, Schweickert A, Blum M. ATP4a is required for Wnt-dependent Foxj1 expression and leftward flow in Xenopus left-right development. Cell Rep. 2012; 1:516–27. [PubMed: 22832275]
48. Walentek P, et al. A novel serotonin-secreting cell type regulates ciliary motility in the mucociliary epidermis of Xenopus tadpoles. Development. 2014:1–8.10.1242/dev.102343
49. Vladar, EK.; Brody, SL. Methods Enzymol. Vol. 525. Elsevier Inc; 2013. Analysis of ciliogenesis in primary culture mouse tracheal epithelial cells; p. 285-309.
50. Hgenlocher C, Walentek P, M Ller C, Thumberger T, Feistel K. Ciliogenesis and cerebrospinal fluid flow in the developing Xenopus brain are regulated by foxj1. Cilia. 2013; 2:12. [PubMed: 24229449]

Author Manuscript Author Manuscript Author Manuscript Author Manuscript

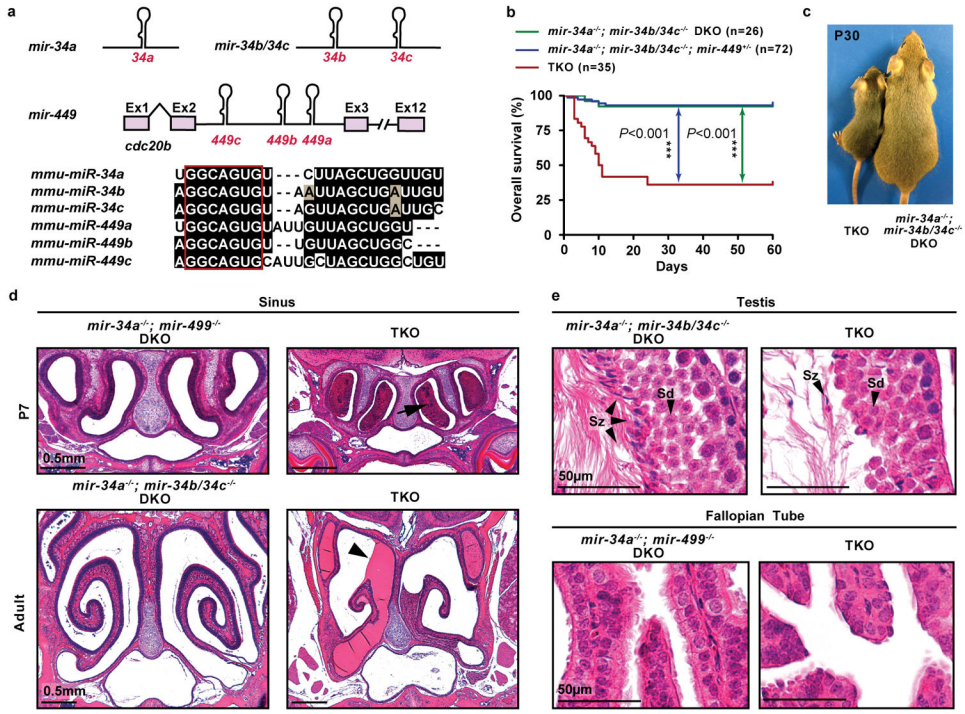

Figure 1. ***miR-34/449*** **TKO mice exhibit defective mucociliary airway clearance and infertility**

a. Gene structure (top) and sequence alignment (bottom) of mouse *miR-34/449* miRNAs. Red box: seed sequences. **b.** TKO mice exhibit frequent postnatal mortality. Log-rank test. **c.** Surviving TKO mice display postnatal growth retardation. **d**. Excessive mucus accumulation and infection in paranasal sinuses of dying TKO at P7 (top) and surviving adult TKO mice (bottom). Arrow: infection; arrowhead: mucus accumulation; n=15. **e.** Adult TKO males and females are infertile. Although early spermatids (Sd) are developed, few intact spermatozoa (Sz) are generated (top, n=3). A significant MCC reduction is observed in TKO fallopian tubes (bottom, n=3).

Author Manuscript Author Manuscript Author Manuscript Author Manuscript

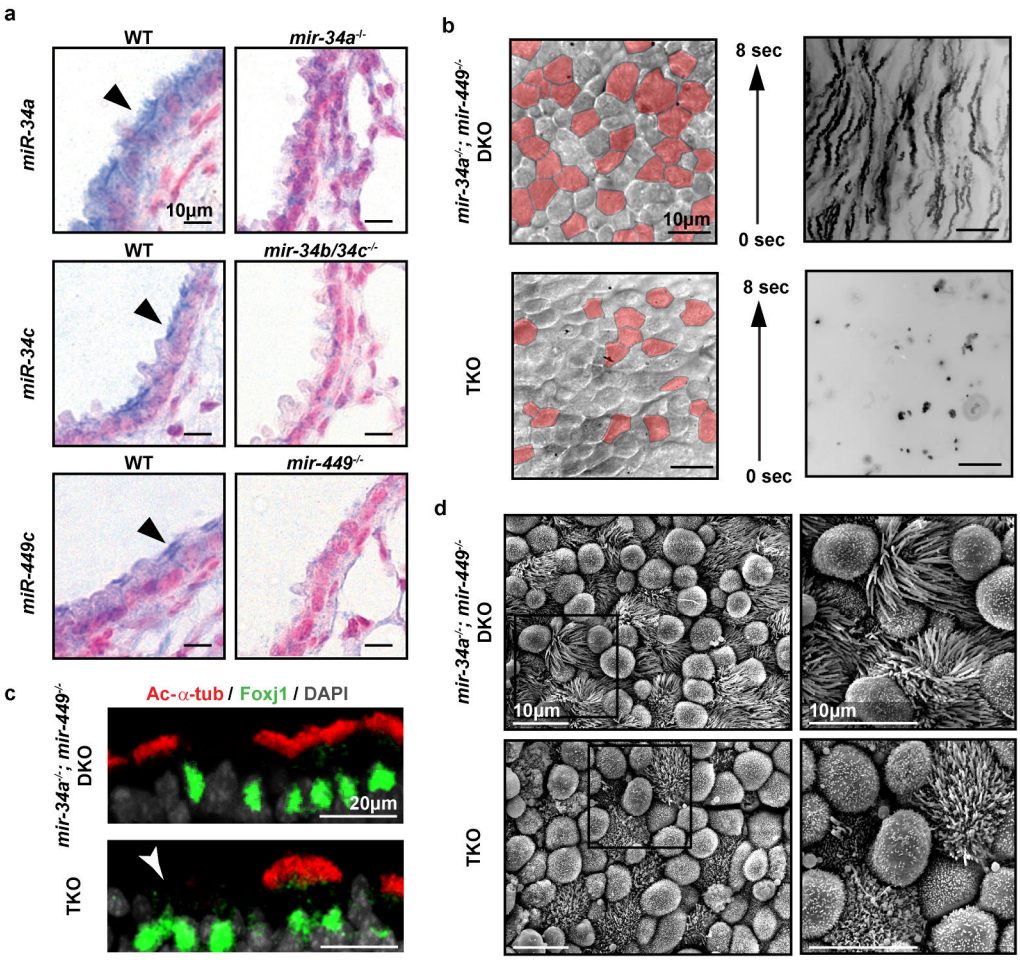

Figure 2. *miR-34/449* deficiency causes ciliogenesis defects in respiratory MCCs

a. *miR-34/449* are strongly enriched in MCCs of respiratory epithelia (arrowheads), shown by *in situ* hybridization. n=2. **b.** TKO tracheal epithelia exhibit defective mucociliary clearance demonstrated by live imaging of fluorescent bead transport. Red: visibly ciliated MCCs; n=4. **c.** Cell-fate specification of MCCs is unaffected in TKO tracheas. Immunofluorescence staining for Foxj1 (a MCC marker) is unaltered in TKO tracheas, yet a large number of Foxj1-positive MCCs (arrowhead) have decreased staining for Ac-α-tub (a cilia marker). n=3. **d.** TKO tracheal MCCs have a significant reduction in cilia number and length, revealed by scanning electron microscopy. n=3.

Author Manuscript Author Manuscript Author Manuscript Author Manuscript

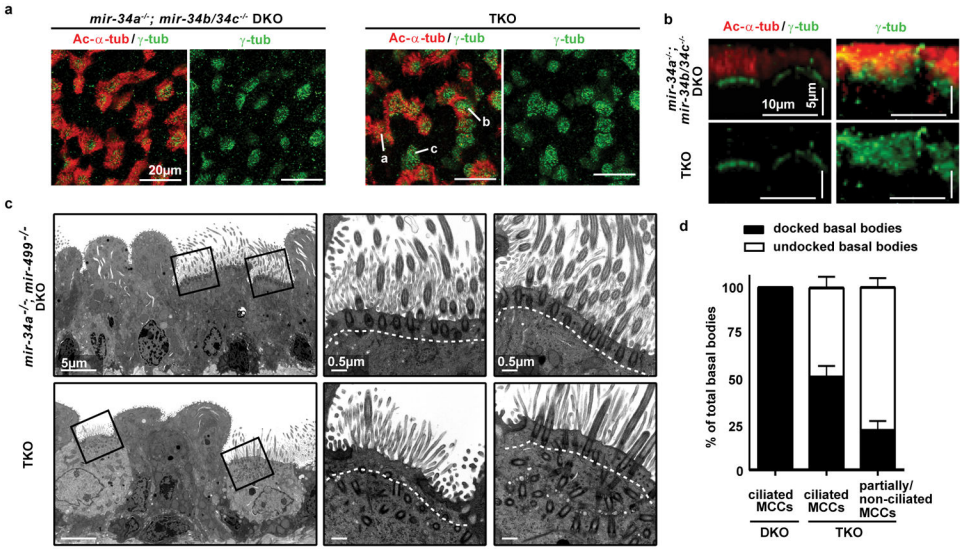

Figure 3. *miR-34/449* deficiency causes defective basal body docking in mouse airway MCCs

a. TKO tracheas exhibit ciliation defects, shown by immunofluorescence staining for Ac-α-tub (cilia) and γ-tubulin (basal bodies). a: fully, b: partially, c: non ciliated MCC; n=3. **b, c, d.** Basal bodies fail to dock to the apical membrane of TKO MCCs. **b.** Lateral projections of confocal micrographs shown in (**a**) **c.** Transmission electron microscopy (TEM) confirms basal body docking defects in TKO MCCs. n=3. **d.** Quantification of basal body docking based on TEM studies in (**c**). Docked and undocked basal bodies exhibit a distance ≤ 0.3 μm and > 0.3 μm to the apical membrane, respectively. Error bar, s.e.m.

Author Manuscript Author Manuscript Author Manuscript Author Manuscript

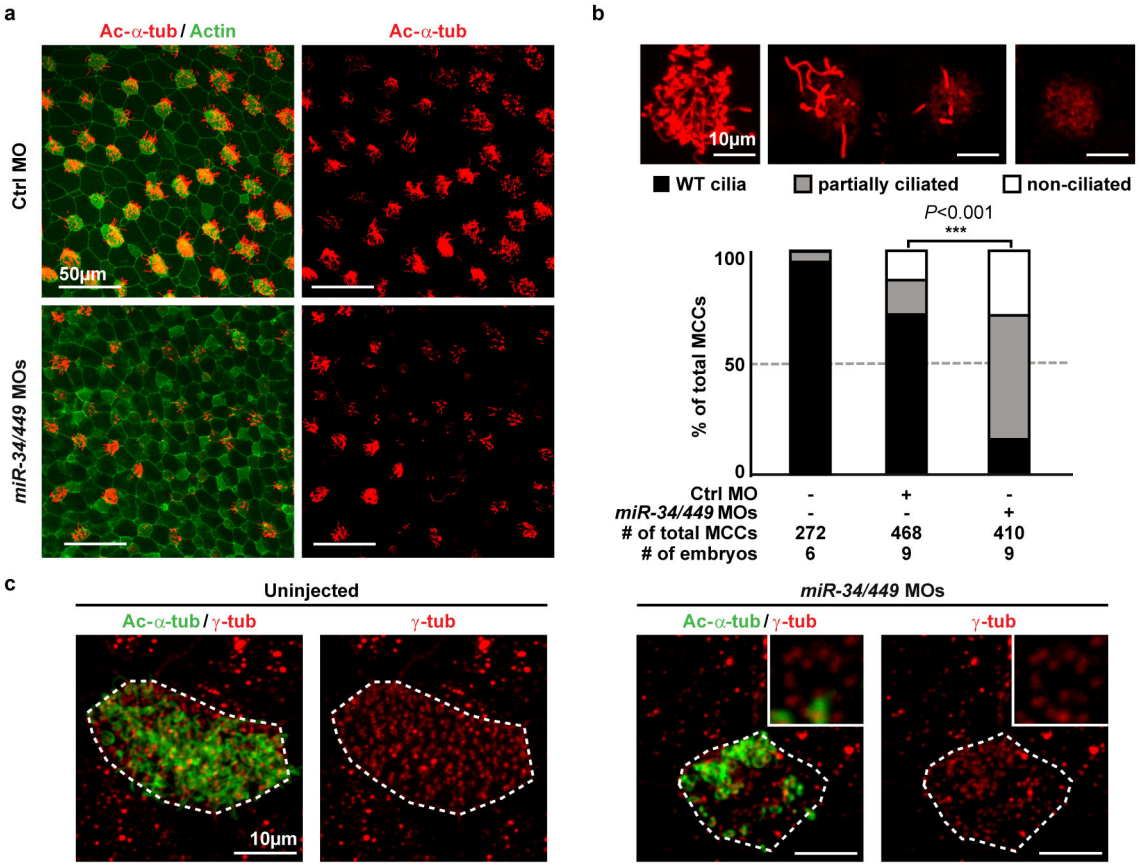

Figure 4. *miR-34/449* deficiency causes defective ciliogenesis in the *Xenopus* embryonic epidermis

a. MCCs in *miR-34/449* morphants show reduced cilia length and number, demonstrated by immunofluorescence for Ac-α-tub (cilia) and phalloidin-488 (Actin). **b.** Quantification of MCC ciliation in (**a**). χ^2-test. **c.** Co-staining of Ac-α-tub (cilia) and γ-tub (basal bodies) in *miR-34/449* morphants reveals uneven/aggregated distribution of basal bodies, which frequently fail to form cilia. Embryos/cells analyzed: Uninjected (4/14), *miR-34/449* MOs (5/30). Embryos were derived from at least two females and independent fertilizations per experiment. Error bar, s.e.m.

Author Manuscript Author Manuscript Author Manuscript Author Manuscript

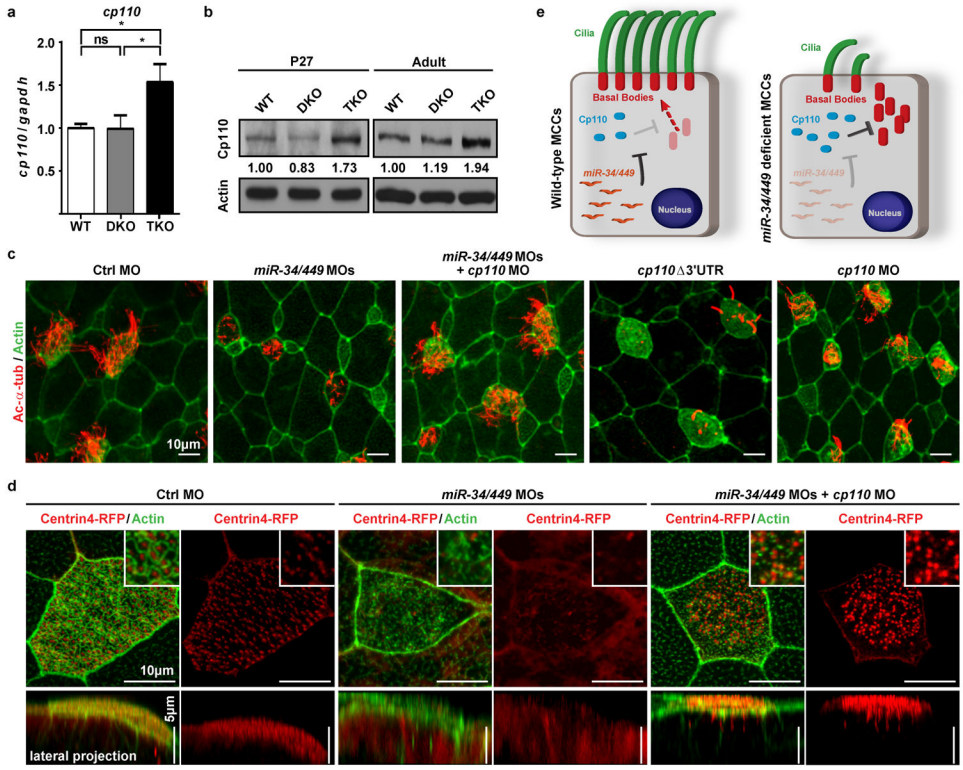

Figure 5. *miR-34/449* miRNAs are required for ciliogenesis by repressing *cp110*

a. *cp110* mRNA is derepressed in TKO tracheal epithelia (n=4). Paired *t*-test, ns $P>0.05$, * $P<0.05$; error bars, s.e.m. **b.** Cp110 protein is elevated in TKO tracheal epithelia. n=3.**c, d.** *miR-34/449* represses *cp110* to regulate MCC ciliation and basal body maturation and docking. **c.** Co-injection of *miR-34/449* and *cp110* MOs rescues MCC ciliation, whereas *cp110*Δ3′UTR overexpression phenocopies *miR-34/449* morphants. *cp110* MO alone also induced ciliation defects. Ac-α-tub: cilia, phalloidin-488: Actin. (Quantification: Extended Data Figure 8b.) **d.** Basal body maturation/docking is reestablished in *miR-34/449* morphants upon *cp110* knockdown. Basal bodies: Centrin4-RFP, Actin: phalloidin-488; Insets: subapical Actin meshwork. Embryos/cells analyzed: Ctrl MO (2/3), *miR-34/440*MOs (5/10), *miR-34/449* MOs + *cp110* MO (4/7). Embryos were derived from at least two females and independent fertilizations per *Xenopus* experiment. **e.** Proposed Model of regulatory role of *miR34/449* during MCC ciliogenesis through direct repression of *cp110*.